NASA CR - 132370

MEASUREMENT AND ANALYSIS OF FORCE-TIME OUTPUTS OF PYROTECHNIC NUTS

by Vernon H. Neubert

Prepared under Contract No. NAS 1-12045 in
The Department of Engineering Mechanics
The Pennsylvania State University
University Park, Pa. 16802

for

NATIONAL AERONAUTICS AND SPACE ADMINSTRATION

CONTENTS

Page

FIGURES

Page

MEASUREMENT AND ANALYSIS OF FORCE-TIME OUTPUTS OF PYROTECHNIC NUTS

SUMMARY

The primary purpose of the study was to compare the dynamic loadings produced by two standard pyrotechnic nuts with loadings produced by four recently developed low-shock nuts. The nuts were manufactured by separate groups under contract with NASA Langley. Each nut was given a number designation, the number having no special significance.

The results show that the use of the Hopkinson bar to measure force-time outputs of the nuts at stud and housing sides aided greatly in understanding the events occurring in the nuts. Acceleration data appear to be dependable, for the most part, but of more limited value.

The low-shock designs show considerable improvement over the standard designs above 4,000 Hz when the results are plotted in shock spectrum form. They involve some penalties with regard to weight and cost.

It is speculated that some of the nuts might produce local structural damage in light structures. They are more likely to cause malfunction of electronic equipment which may be mounted nearby. This should be studied further.

INTRODUCTION

The purpose of the work summarized herein was to assist in construction and calibration of a pyrotechnic shock monitoring apparatus, and to analyze the data produced by the apparatus. The apparatus was constructed at the NASA Langley Research Center.

The apparatus constructed was similar to that developed by the author under a previous NASA Grant (Reference [1]) to measure the output of explosive bolts. The support furnished under the present contract was to consist primarily of the following:

(1) Make recommendations regarding strain gauges, strain gauge amplifiers, associated mounting fixtures, and suggestions on separation nut mounting adaptors.

(2) Assist in the initial tests. The preliminary tests involved impacting metal spheres with known impact characteristics against the end of the bar to assure that the apparatus was operating satisfactorily. This accomplished, a series of seven different pyrotechnic nuts were tested by NASA personnel using the apparatus.

(3) Accomplish dynamic analysis of test results as follows:

    (a) To attempt to match the force-time records obtained with the actual events of the nuts' separating mechanisms.

    (b) To postulate on the effects of the mechanical shocks on spacecraft structures.

    (c) To compare the performance of the various nuts, comparing advantages and disadvantages of each type.

During the period of the contract, a technical paper, Reference [2], was published providing basic performance comparisons of seven separation nuts. For the present report, the "APPARATUS" section and the subsection entitled "Functioning of Nuts" under "PROCEDURE" are quoted from Reference

[2] and were written by L. Bement. Also, figures 1 through 21 are exactly the same as those used in Reference [2]. Thus, to accomplish the assigned task of summarizing results, the author has included reference to much of the work done at NASA Langley.

APPARATUS

The experimental apparatus consists of the montoring system and seven separation nuts.

Monitoring System

The main elements of the monitoring system shown in Figure 1 are the two 12-foot long, one-inch diameter, cold rolled steel bars that were hung by 36-inch cables. The shock waves generated by the separation nuts travel in a uniform plane wave down the bar at sonic velocity. Therefore, a time period of 1.44 milliseconds is required for a wave to traverse the 12-foot length and return to its source, allowing a pulse within that duration to be viewed as a single pulse. The principles of shock waves in uniform, thin bars are explained in detail in Appendix A.

Several adaptors were machined to accommodate the stud thread sizes, 7/16-20 or 1/2-20, and lengths. Also, a cylindrical adaptor with a half-inch wall was machined to allow the monitoring of shock waves through the flange of the separation nuts. All separation nuts, except Low Shock Design 4, utilized this adaptor. Low Shock Design 4 had no mounting flange, and the bar was threaded into a tapped portion of the nut's cap. This technique considerably improved the coupling of the nut's generated shock over the

flange mounted approach. An eighth-inch, 3.2 inch diameter flat-washer was installed at the nut to stud interface to simulate the fixed surface of a typical spacecraft system.

The shock waves were monitored by strain gauges and accelerometers at positions indicated in Figure 1. The strain gauges were mounted on diametrically opposing positions on the bars and were wired within the Wheatstone bridge of the amplifier to cancel the effects of longitudinal bending of the bars. The gauges, Baldwin Model FAB1235S13, and the amplifiers, Ellis Model BAM-1B, have a frequency response flat to at least 100 KHz. The accelerometers, Endevco Model 2225C, have a resonant frequency of 80 KHz and a mounted resonant frequency of approximately 50 KHz, yielding a monitoring capability that is flat to 10 to 16 KHz. The accelerometer amplifiers are Endevco Model 2718.

The dynamic pulses were recorded on an FM magnetic tape recorder with a frequency response flat to 40 KHz (capable of measuring rise times to six microseconds). The equivalent paper speed of the permanent records, achieved by reducing playback speeds, was over 2200 inches/second, or 0.48 milliseconds/inch.

Separation Nuts

The performance of seven separation nuts was evaluated in this program: a non-captive design which was historically the first and simplest release nut concept, two "Standard" designs that have been utilized considerably in present and past aerospace programs, and four "Low Shock" designs that were specifically designed toward reducing the mechanical shock generated on actuation. Although each nut could contain two cartridges for redundancy, only

one cartridge was used for each functioning.

The following explanations describe only principles. Physical designs and performance margins are beyond the scope of this presentation.

Non-captive - See Figure 2. The bolt is retained by the threaded portion of the steel collet which is in four segments. The segments are in turn held in position by a retaining ring. Electrical ignition of the gas generating cartridge, which produces 1000 psi in a 10 cc closed volume, pressurizes the volume formed by the bolt end and the housing. The housing is forced to the right, stripping back the retaining ring and releasing the collet segments. No effort is made for confinement of gases, housing, or collet segments.

Standard Design 1 - See Figure 3. This release mechanism is similar to that of the non-captive nut; the retaining cylinder holds the collet assembly at its base and is withdrawn. The collet in this design has four deep incisions, instead of being segmented. The SBASI (Single Bridgewire Apollo Standard Initiator), which produces 650 psi in a 10 cc volume, pressurizes the volume formed by the piston and the retaining cylinder, causing the cylinder to stroke to the right. The piston holds the nut segments in position. As the restraining ring strokes over the collet, the flared portion of the collet is compressed, forcing the base of the collet to petal open, hinging at the base of the incisions, and releasing the bolt. The restraining piston is decelerated by the o-ring as it impacts against the housing.

Standard Design 2 - See Figure 4. The retaining cylinder holds the segmented collet at two circumferential points of increased diameter. The spreader piston is spring loaded to restrain and spread the segmented collet

on its release. The cartridge, which produces 1400 psi in a 10 cc volume, pressurizes the volume formed by the housing and the top of the restraining cylinder. This forces the restraining cylinder to the left, allowing the four collet segments to fall into the cylinder's recessed areas, releasing the bolt.

Low-Shock Design 1 - See Figure 5. This nut is a modification to Standard Design 1 and utilizes the same release mechanism; the restraining cylinder strokes to the right on pressurization from the output of a SBASI, compressing the incised collet. The shock reduction principles were to use an increased mass for the pistons to minimize their acceleration and to maximize the restraining cylinder's acceleration, and to use crushable honeycomb to reduce the peak load forces on the piston and retaining cylinder from the brisant output of the SBASI. This would reduce the pressure-induced loads through the collet into the bolt. The outer honeycomb provides for a longer period of deceleration on impact.

Low-Shock Design 2 - See Figure 6. The output of the SBASI cartridge is ported into the body of the nut to force the restraining cylinder to the right, releasing the three-segmented collet. The deceleration of the retaining cylinder is achieved by compressing gases in the cavity formed by its outer face and the housing.

Low-Shock Design 3 - See Figure 7. The output from the SBASI cartridge is ported through the body of the hinging piston to force the retaining cylinder to the right. As the retaining cylinder strokes, the three-segmented collet is first released at its base and is then forced to rotate open about the hinging piston by contacting the lower lip of the recessed area in the retaining cylinder. The low shock principles were to use a high mass piston

and have all mechanical energy to be dissipated in the internal components without decelerating against the housing.

Low-Shock Design 4 - See Figure 8. The output of the cartridge, which produces 2,360 psi in a 10 cc closed volume, is ported to the annular ports at each end of the nut body. The two retaining cylinders are forced inward, allowing the three-segmented collet to fall into the recessed areas under the force of an expansion spring (not shown). The shock reduction principles were to avoid loading the bolt from the cartridge output, and to have the low-mass retaining cylinders dissipate their energy on impacting together, rather than against the housing.

PROCEDURE

The total study involved:

1. Establishing and calibrating a monitoring apparatus.
2. Functioning six separation nuts.
3. Analyzing performance records to attempt to match records with events occurring during separation.
4. Postulating on the effects of the shocks on spacecraft structures and systems.
5. Comparing performance of the various nuts.

Calibration of Monitoring Apparatus

The bar used in the monitoring apparatus is described in the previous section. The response of this bar to a longitudinal impact with a steel ball is fairly well known. The bar was therefore impacted with a 1.50 inch diameter hardened steel ball, supported on a 60 inch pendulum, with horizontal pull-backs of 12, 24, and 36 inches from the end of the bar. The pulse produced in the flat-ended cylindrical bar was then compared with that produced using several different end adaptors. Three end adaptors were used: (1) cylindrical, 1-1/2 inches long and 1 inch in diameter; (2) tapered, from 2 inches diameter to 1 inch diameter, and 1-1/2 inches long (short taper); and (3) tapered, from 2 inches diameter to 1 inch diameter, and 4 inches long (long taper).

All interfaces were coated with silicone grease to assure good contact. During initial tests, strain gauges were monitored individually to determine possible eccentricities in loading.

The non-captive nut was tightened onto the stud and functioned during the calibration phase using only the one bar (Figure 1), since there was no housing attachment. A torque of 100 in.-lb. was used.

Functioning of Nuts

The six separation nuts were functioned first under torques of 100 in.-lb. on the stud monitoring bar. The housing flanges (except for Low-Shock Design 4) were bolted to the housing monitoring bar. The number of nuts of each type functioned under this arrangement was: six each of Standard Designs 1 and 2, six each of Low-Shock Designs 1 and 4, and one each of Low-Shock Designs 2 and 3. One of the primary purposes of the tests was to attempt to associate events in the force-time history with mechanisms of the functioning nuts.

To determine the effect of torque, three additional nuts were functioned at 600 in.-lb. and 900 in.-lb. using both bars; They were Standard Design 1, Low-Shock 1, and Low-Shock 4. The non-captive nut was also tested at these levels using the single bar. Results are reported in Reference [2], but not duplicated herein.

To determine the effect of restraint from the stud monitor, five nuts (all except Standard Design 2) were functioned with a free stud on the nut, that is, without the stud monitoring bar. This was to simulate the situations in which the nut housing is secured to the structure and the stud is allowed to move. Results are reported in Reference [2].

For many of the tests the rigid-body motion of the monitoring bars was observed with a 400 pps framing camera. The rigid-body motion is associated with the net impulse delivered to the end of each bar.

Performance Analysis

For comparison of performance under 100 in.-lb. torque, the force and acceleration histories of one representative record of each nut type were plotted on the same scales. Also, the net impulsive loads produced by the actuation of each nut type were compared.

The acceleration-time histories of representative records were analyzed on a NASA shock spectrum analyzer (MB Model 980) to 40 Khz with a Q of 10. Only the first pulse produced was analyzed during the period of the pulse itself, for a maximum time of 1.34 milliseconds. Thus the peak response of the single-degree-of-freedom-system could be determined only while the pulse was acting, and the resulting spectrum is a primary spectrum of absolute acceleration.

Typical force-time histories were digitized at 10 micro-second intervals by the author. The response of a single-degree-of-freedom-system with no damping, or $Q = \infty$, was calculated on a digital computer and non-dimensional maxi-max displacement shock spectra plotted. Values were calculated at integral multiples of 384 Hz.

From the digitized force-time data, theoretical acceleration time curves were calculated, to compare with measured acceleration for two nuts by differentiating the strain-time history and multiplying by the factor (2a) as explained in Appendix A. Here "a" is the speed of sound in the measuring bar.

Effects on Spacecraft Structures and Systems

In order to postulate on the effects of the shock on spacecraft systems, the results of some present and past analyses and experiments conducted by

the author and others are considered. The analysis of actual portions spacecraft structure or equipment should be the next phase in the study as originally proposed in Reference [6]. Under the present scope of work, it was only possible to analyze a beam-like strip of shell.

Comparison of Performance of Various Nuts

The performance of the various nuts is compared, to summarize results. Trade-off in gains in weight and size of the low-shock nuts is discussed.

RESULTS

Calibration of the Monitoring Apparatus

The theory of the behavior of stress waves in the monitoring bars is discussed in detail in Appendix A. Typical signals from the strain gauges and the accelerometer are shown in Figure 9. The strain ε is converted to force by multiplying the measured strain by AE, the bar area times Young's Modulus for steel. The stress σ can be obtained by dividing the force by A, which was 0.785 square inches. Compression is down on the force time records. It can be seen from the record for a 12 inch horizontal displacement of the steel sphere that a compressive wave first passes the strain gauge station, which is 10 inches from the impacted end. It is reflected as a tensile pulse which passes the strain gauge about 1.34 milliseconds after the first compressive pulse. The wave then travels 10 inches to the struck end and is reflected as a compressive wave. To travel the 20 inches requires only about 100 microseconds. Since the pulse is about 118 microseconds long, the tail of the first tensile pulse overlaps the beginning of the second compressive pulse, and there is some cancellation. However, there is an interval of about 1.34 milliseconds, before any reflection appears, which can be used to observe the primary pulse.

As the ball displacement increases to 36 inches, the pulse shortens to about 90 microseconds. It should be noted that the pulse maintains the same shape and magnitude as it travels along the bar, which is the ideal situation for measurement.

As indicated in Appendix A, the acceleration at the bar end would be

equal to the factor (2a) times the derivative of the strain with respect to time at the strain gauge station. The force or strain pulse is approximately a haversine, so there are two acceleration peaks and the acceleration pulse is about twice the frequency of the force pulse. The high frequency signal on the acceleration pulse may be a slight ringing of the accelerometer.

The short taper adaptor had no appreciable effect on the pulse shape or duration, so a 45^{0} angle was used for the housing adaptor. The long taper adaptor caused the pulse to be attenuated by about 15 per cent and was considered unsatisfactory.

Typical performance plots for the noncaptive nut are shown in Figure 10. The only active force initially is that due to the pressure from the cartridge. While there is initial compression on the end of the stud, the housing is being forced away from the stud, tending to cause tension in the outer surface of the bar due to friction and shearing of a pin between the retaining ring and collet (see Figure 2). The tension apparently dominates until the pin is sheared. Then the pressure within the cavity continues to load the stud until the stud is released. It would be difficult to identify the events on the acceleration record. The rigid body displacement of the bar and net impulse are discussed in Reference [2] and are not repeated here. The bar swing is about 10 inches.

Functioning of Nuts

The discussion of the performance of each nut is taken from Reference [2]. The timewise records were found to be quite reproducible for nuts of a certain type, so only one of each typical record is included.

Standard Design 1. - See Figure 3 for the cross section and Figure 11 for the functional histories. As the retaining cylinder is forced to the right, a momentary tensile wave is created in the bolt. This is followed by a strong compressive force produced by the piston against the collet. The major tensile spike is produced by the retaining cylinder stroking the flared portion of the collet. The housing first experiences a tensile wave as a reaction force to the acceleration of the retaining cylinder applied through the collet. As the retaining cylinder impacts against the O-ring and housing, a strong compressive pulse is produced. The monitoring bars were observed to swing apart by approximately 15.24 cm (6 in.) on functioning.

Standard Design 2. - See Figure 4 for the cross section and Figure 12 for the functional histories. The initial tensile load in the stud appears to be produced by the housing reaction in loading through the collet which exceeds the compressive loading produced by shearing the shear pin between the retaining cylinder and the collet. The large compressive spike is produced by the impacting of the retaining cylinder, bottoming against the housing. The housing load first exhibits a compression corresponding to the reaction to the initial tensile load of the stud. The major shock of the impacting retaining cylinder is apparently transferred efficiently into the stud mass and not the housing. The second compressive load of the housing can be attributed to the bottoming of the spring or spreader piston against the retaining cylinder in ejecting the stud. The positive pulse could be related to the seating of the spreader piston in the then-expanded collet sections. The monitoring bars swung apart approximately 20.32 cm (8 in.) on functioning.

Low-Shock Design 1. - See Figure 5 for the cross section and Figure 13 for the functional histories. The initial tensile pulses on the stud can be related again to the shearing of a shear pin and friction when the retaining cylinder begins its motion. The major compressive indication is caused by the loading through the pistons and honeycomb. The retaining cylinder impacting the flared portion of the collet produces the sharp tensile pulse. The loads into the housing are apparently well isolated from the stud; the reactionary forces are low, reduced by the crushable honeycomb and the acceleration of the high-mass piston. A small tensile load is coupled through the washer at the interface, followed by a compression produced by decelerating the retaining cylinder against the housing. No separation of the bars was observed on functioning.

Low-Shock Design 2. - See Figure 6 for the cross section and Figure 14 for the functional histories. The initial stud compressive load is produced by the force of the spreader piston on the collet on pressurization. The tensile pulse is produced by the friction of the retaining cylinder withdrawing over the collet. The subsequent compressive pulses are then created by the piston-loaded segments sliding outward and bottoming into the cavity to release the bolt. The stud is abruptly off-loaded when the piston is stroked to the right by the internal shoulder of the retaining cylinder. The housing experiences the small compressive pulse due to a pressurization force to the right, followed by the tensile pulse produced by the reaction to the

friction resistance in forcing the retaining cylinder to the right. The next compressive pulse is the reaction to the loading of the collet by the piston. The remaining compressive pulse can be attributed to the deceleration of the retaining cylinder and piston within the housing by the residual gas from the cartridge. The bars swung apart approximately 10.16 cm (4 in.) on functioning.

Low-Shock Design 3. - See Figure 7 for the cross section and Figure 15 for the functional histories. The initial tensile indication on the stud is due to the movement of the retaining cylinder to the right. The hinging piston applies the major compressive load, which is quickly converted to tension when the retaining cylinder's recessed area impacts the projection of the collet. The second compressive pulse can be attributed to the forcing of the combination of hinging piston, retaining cylinder, and collet to the left, and applying a compressive load against the stud. The initial tensile load produced by the housing can be attributed to the reaction to the retaining cylinder's motion to the right. The compressive pulse is the reaction to the loading of the collet. On release of the bolt, the housing load would remain compressive during the deceleration and reversal of the piston/cylinder. A positive pulse would be produced on the impacting of the piston/cylinder against the bottom of the housing. The bars were observed to swing apart approximately 20.32 cm (8 in.) on functioning.

Low-Shock Design 4. - See Figure 8 for the cross section and Figure 16 for the functional histories. The loads by the converging retaining cylinders coupled into the collet, and transferred into the stud, are essentially balanced. The compressive load may be attributable to the relaxation of the long-length stud on release. The major identifiable load produced by the housing is compressive, possibly caused by a pressurization of the port volumes. The force is appreciably higher as compared to the other nuts, due to the mounting of the bar into the nut cap rather than in a flange at its base. No separation motion of the monitoring bars was observed.

Performance Analysis

Comparison of force and acceleration under 100 in.-lb. torque are made in Figures 17 through 19.

It can be seen from Figure 17 that the maximum stud force on Standard Design 2 is much higher than that of all the other designs. The lowest stud force level is indicated for Low-Shock Design 4. The acceleration levels are comparable.

The situation is somewhat different with housing force (Figure 18), in that force levels for Low-Shock 3, for example, are as high as for the Standard Design 2. However, the housing force levels are still small, a maximum of 3110 lb., compared to the stud force maximum of 32,600 lb. As shown in Figure 19, housing acceleration levels are also significantly lower than those at the stud.

The acceleration shock spectra in Figures 20 and 21 show how a single-degree-of-freedom-system, or each mode of a structure, would respond during the time of application of the pulse. The relative positions on the spectra in Figure 20 are about as expected. Standard Design 2 is highest and Low-Shock 4 is lowest at low frequencies, but Low-Shock 1 is lowest at high frequencies.

The spectra obtained from digitized stud forces are shown in Figure 22. The difference between acceleration spectra obtained from acceleration records and the spectra obtained for forces is explained in Appendix B. The values taken from Figure 22 would need to be multiplied by 1 lb./k, where k is the stiffness of the system, or mode, in lb./in. It was found that, except at

384 Hz, the primary spectrum values were higher than the residual spectrum values. Therefore, above this value the maxi-max spectrum and the primary spectrum are the same. At lower frequencies, the pulse is over before the system can reach its peak level, so the peak occurs after the pulse, which is by definition during the residual time interval. The relative positions show the Standard Designs considerably above the Low-Shock Designs.

To help interpret the behavior of the nut mechanisms, the timewise derivative of the stud force was taken from the digitized data. This is of limited accuracy, since the digitizing interval was 10 microseconds. The derivative of the force shows the maximum rate of force build-up, from pressure or impact, or relief, say from shearing a pin. In Figure 23, the maximum rate of stud-force build-up for Standard Design 1 is about 270×10^6 lb./sec. and the maximum rate of force relief is -160×10^6 lb./sec. Note that

$$\frac{1}{AE} \frac{\partial F}{\partial t} = \frac{\partial \varepsilon}{\partial t}$$

Also, from Appendix A, Equation (A-9)

$$\text{acceleration} = \frac{\partial^2 u}{\partial t^2} = a \frac{\partial \varepsilon}{\partial t}$$

$$\text{then} \quad \frac{\partial^2 u}{\partial t^2} = \frac{a}{AE} \frac{\partial F}{\partial t}$$

$$\text{or, in "g",} \quad \frac{1}{g} \frac{\partial^2 u}{\partial t^2} = \frac{a}{AEg} \frac{\partial F}{\partial t}$$

$$\frac{1}{g} \frac{\partial^2 u}{\partial t^2} = 23.3 \times 10^{-6} \frac{\partial F}{\partial t}$$

Therefore, the acceleration-time curve should be the same shape as the $\frac{\partial F}{\partial t}$ curve and a separate scale of bar acceleration is given in Figures 23 and

24. As explained in the Appendix, the accelerations at the end of the bar are double those at the center, due to the end reflection.

It is of interest to compare the accelerations predicted from strain measurements (Figure 23) with those measured (Figure 11). Note that the first peak predicted is, as expected, about half that measured, that is 6300 g compared to 12,900 g. A single predicted peak then occurs immediately in the opposite, while many occur in the measured acceleration at a frequency of about 50,000 Hz. This is equivalent to a wave length in the bar of four inches, which should be sensed by the strain gauges.. It may be ringing of the accelerometer, but it damps out more rapidly than would normally be expected in an accelerometer. Note that the same phenomenon occurs at 0.300 milliseconds. It is most likely due to impacting of the accelerometer casing on the bar end caused by the sharp tensile force. The accelerometer was attached to the end of the bar by a threaded stud. The stud is put into tension as the accelerometer is tightened, while the contact surface between the accelerometer and the bar end is in compression. If this compression preload is exceeded during a test, the accelerometer casing will lose contact with the end of the bar. The stud tension will momentarily increase and the stud will act as a spring to pull the accelerometer into contact again, probably with a local impact or shock occurring.

Similarly, the acceleration in Figure 24 may be compared with that for Standard Design 2 in Figure 12. Here there are no extraneous peaks in the measured acceleration, and the magnitudes are in reasonable comparisons.

Effects on Spacecraft Structures and Systems

The measured force levels allow one to do some general speculation about damage to structures that would not be possible with measured accel-

erations. Using Standard Design 2 as an example, a 32,600 lb. pulse occurs which lasts about 60 microseconds. This stud force is delivered over a relatively small area, and there may be a possibility of local bearing or punching shear damage to thin plating. For structural members of 1/2 square inch or more, which are in tension or compression, the stress levels would be tolerable. For shell plating in bending, it is more difficult to speculate. As an admittedly over-simplified example, a strip of reinforced plating was analyzed as shown in Figure 25. The plating taken was 2 inches by 0.0625 inches reinforced by a cross-section 1/2 inches by 0.125 inches.

For one example, the strip was taken as a hinged-hinged beam 88.62 inches long. To simplify the analysis, the beam was loaded by a triangular pulse, as shown, of magnitude P_o and duration t_o. In Figure 26, the bending moment M at the center-line is given as $M|P_o\ell$ versus time for t_o = 60 microseconds and t_o = 300 microseconds. The theory used is for a Bernoulli-Euler beam and is summarized in Appendix C. Taking P_o = 32,600 lb. for the dominant stud pulse for Standard Design 2, then the maximum moment is about (0.00145)(32,600)(88.6) = 4188 in-lb. and the maximum bending stress would be 1,073,000 psi. For the 300 microsecond pulse, with the P_o = 5320 lb. peak from Standard Design 1, the peak value of M from Figure 26 would be (0.0035)(5320)(88.6) = 1650 in.lb. or a peak bending stress of 423,000 psi.

The maximum value of $M|P_o\ell$ depends on ℓ. In another example, for a 20 inch beam of the same cross section, the maximum value of $M|P_o\ell$ for the 60 microsecond pulse was 0.0072. The maximum moment for Standard Design 2 would then be (0.0072)(32,600)(20) = 4694 in.lb., which is slightly greater than for the beam of length 88.6 inches.

These bending stresses are quite high. In an actual spacecraft plate

or shell theory should be used. Also, in applications, it is not likely that a nut would be used without some reinforcement of the local structure to support an attachment. The level of effort involved did not allow for further analysis. However, it can be said that the loadings are sufficiently severe that local damage could occur to very thin structures.

Comparison of Performance of Various Nuts

The nuts are compared in plots of force-time outputs, acceleration-time outputs, acceleration shock spectra, and displacement shock spectra in the previous section, Performance Analysis. On shock spectra from measured stud forces (Figures22), the low-shock designs are clearly superior between 4,000 and 24,000 Hz, with Low-Shock 4 the best. Below 4,000 Hz, Low-Shock 1 approaches Low-Shock 4, and Standard 1 is very close to Low-Shocks 2 and 3. In acceleration spectra in the stud side, Low-Shocks 1 and 4 are very close between 4,000 and 24,000 Hz. The standard Design 1 is very close to Low-Shock 3 in the same range, with Standard 2 considerably higher. On the housing side (Figure 21), in the same frequency range, Low-Shocks 1 and 2 are best. Below 4,000 Hz, Low-Shock 1 is highest on the housing side.

In summary, it is difficult to make a direct overall comparison. One must consider frequency range of interest, and stud and housing loading. Also, on structures, force may be more important--on equipment the base acceleration may be more directly useful. In general, it can be said that the low-shock designs show a considerable decrease in loading compared to standard designs.

CONCLUSIONS AND RECOMMENDATIONS

The initial calibration of the monitoring apparatus involved using steel spheres with relatively small inputs compared to some of the nuts. During this phase of the study it was shown that the housing adaptor used would have a minimum effect on the measured pulse shape. During tests with the nuts themselves, calculations indicate the stresses in the measuring bars remained in the elastic range. Some dispersion of the axial stress wave occurred for very sharp pulses, but this effect was minimized by measuring strains only 10 inches from the nut. The accelerometers appeared to follow the response accurately to higher frequencies than expected. Some slight impacting of the accelerometer on the stud force measuring bar may have occurred due to the severe tensile loads produced, for example, by Standard Design 1 and Low-Shock Design 1. See the discussion on page 18.

Little can be said about the functional performance of the nuts. For low-frequency improvement, porting of gases to aid in deceleration of mechanical parts might be preferable to use of honeycomb, which tends to spread the impact over a longer period of time. Careful study of force-time records might show the designer how to improve various nut designs.

The performance evaluations and analyses show that, in general, the low-shock designs result in a considerable reduction in force and acceleration levels when compared with the standard designs.

In addition to the direct axial force from the nut, a moment could be produced if the axial force is applied eccentrically to the stud bar. This would result in bending of the measuring bar, as discussed in Appendix A. For some tests, strain gauges 20 inches from the end of the bar were used to measure bending. For Standard Design 2, the peak bending strain was 130 μ in./in., which was about 10 per cent of the peak axial strain. The associated moment would be about 380 in.-lb. for the measuring bar at that point. Although a more thorough analysis would need to be done for an accurate estimate, this value of moment indicates an effective eccentricity of about r|40, where r is the bar radius, or less than 0.02 inches. For Low-Shock Design 1, the peak bending strain was about 25 per cent of the peak axial strain, for an effective eccentricity of about r|16, more than twice that of Standard Design 2.

The shock spectra represent the peak response of a single-degree-of-freedom-system to the loadings. As such, they are most useful in predicting response of equipment within spacecraft and near the pyrotechnic nut. Some electronic equipment may be seriously damaged by 43,000 g, even though the duration at this level is very short. The low-shock designs produce lower g levels, but of longer duration. The shock spectrum in Figure 20 shows that below 400 Hz, some of the low-shock designs may produce more severe loading on equipment than the standard designs.

The effects on spacecraft and systems should be the subject of a special study. Now that some idea has been obtained as to the timewise variation of loading from some pyrotechnics, the next step should be to carry out experiments and related analyses on the effects of the devices on more realistic, if ideal, structures. One of the most severe pyrotechnic events occurs during the separation of two stages of a rocket. This could be simulated using shells which are appropriately instrumented.

From the present study of nut outputs, it appears that local structural damage could be produced by a nut if it is placed at an un-reinforced point on a shell--which is not likely. It is more likely that electronic equipment located near a pyrotechnic nut might be damaged. Results indicate that both an axial force and a moment are produced by the nuts, although the axial force received the most attention in this study and appears to be the most important.

No conclusions can be stated with respect to choice of one nut over another for a specific application. Cost, simplicity of operation, and weight are important factors--in addition to loading produced. In some cases, it may be acceptable to use Standard Design 2 even though it produces the highest loads and accelerations. Frequency range, as well as housing versus stud force and acceleration levels may be important factors in choosing the best nut for a particular application.

REFERENCES

1. V. H. Neubert and R. P. Parker, "High Frequency Shocks of Spacecraft Systems," Final Report, NASA Contract NGR 39-009-146, November 24, 1971.

2. L. J. Bement and V. H. Neubert, "Development of Low-Shock Pyrotechnic Separation Nuts," Proceedings of the Eighth Aerospace Mechanisms Symposium, NASA Langley Research Center, October 18, 1973.

3. S. Timoshenko and J. N. Goodier, Theory of Elasticity, second edition, McGraw-Hill Book Co., Inc., New York, 1951, pp. 383-4.

4. R. P. Parker, "High Frequency Response of Bars and Beams," Ph.D. Dissertation, Department of Engineering Mechanics, The Pennsylvania State University, March, 1973.

5. J. P. Jent, "Longitudinal-Flexural Bar Vibrations Due to an Axial Eccentric End Impact," M. S. Thesis, Department of Engineering Mechanics, The Pennsylvania State University.

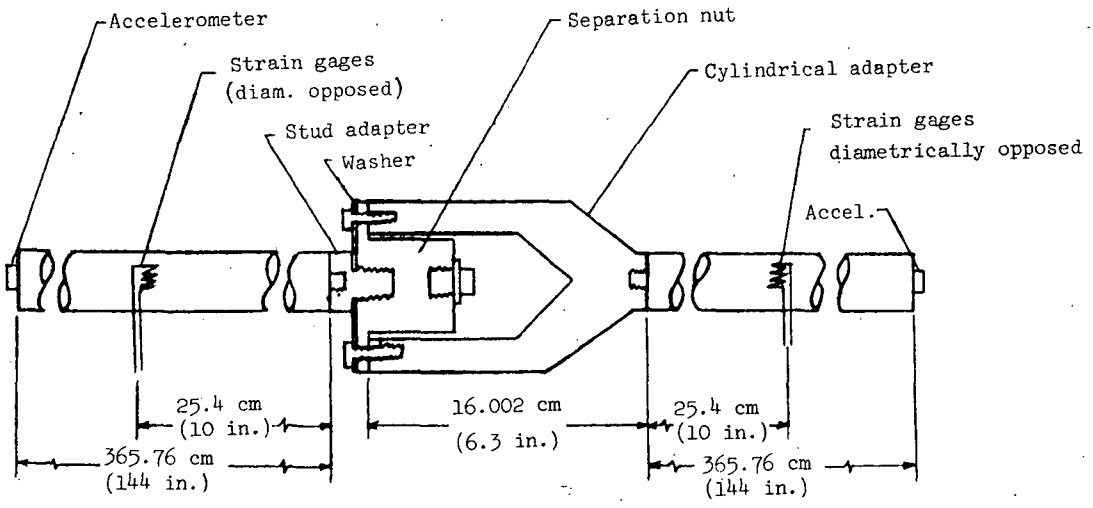

Figure 1.- Cross section of shock monitoring apparatus.

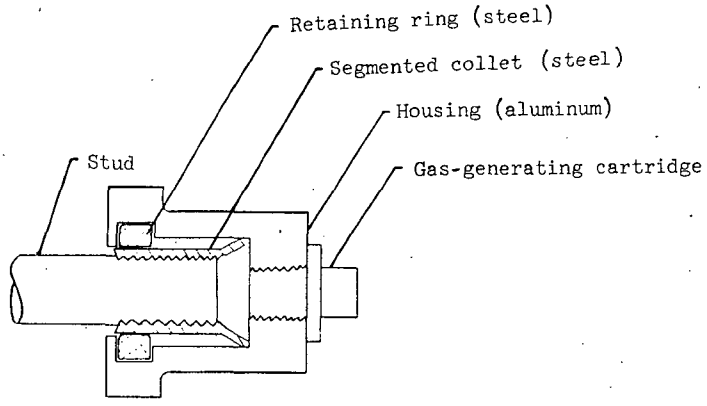

Figure 2.- Cross section of noncaptive separation nut.

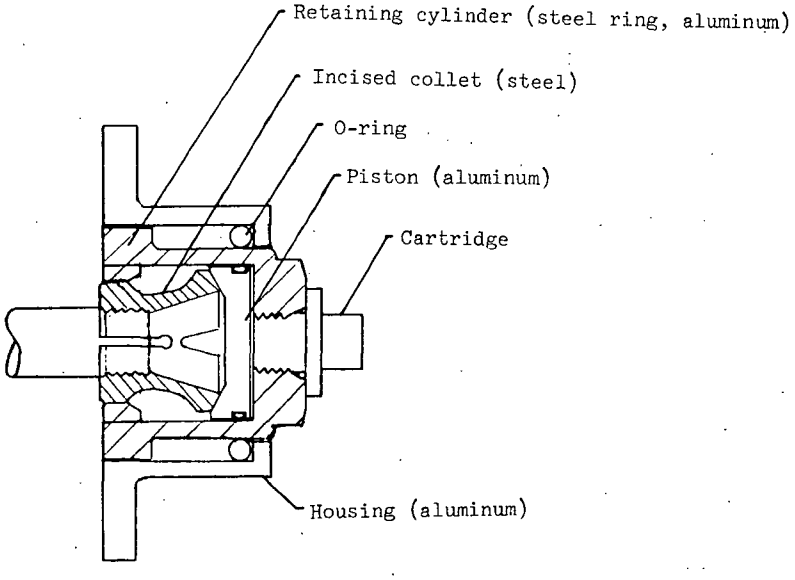

Figure 3.- Cross section of Standard Design 1.

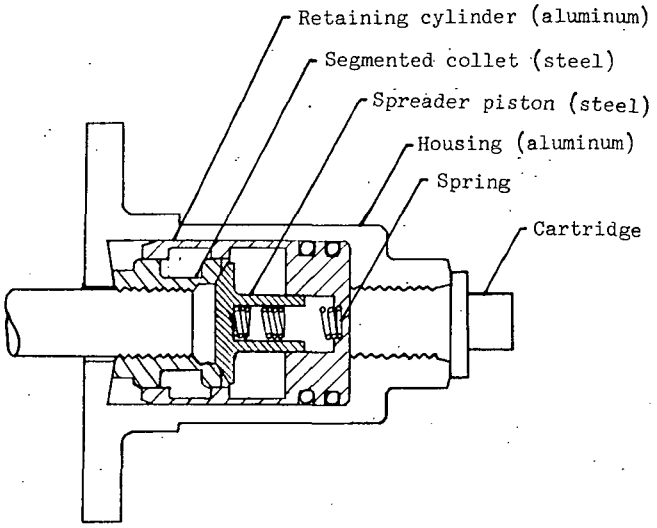

Figure 4.- Cross section of Standard Design 2.

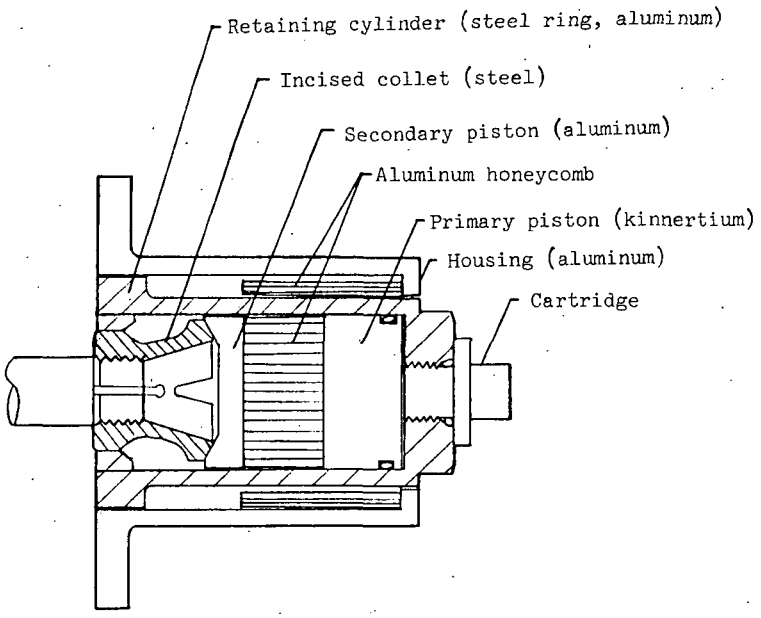

Figure 5.- Cross section of Low-Shock Design 1.

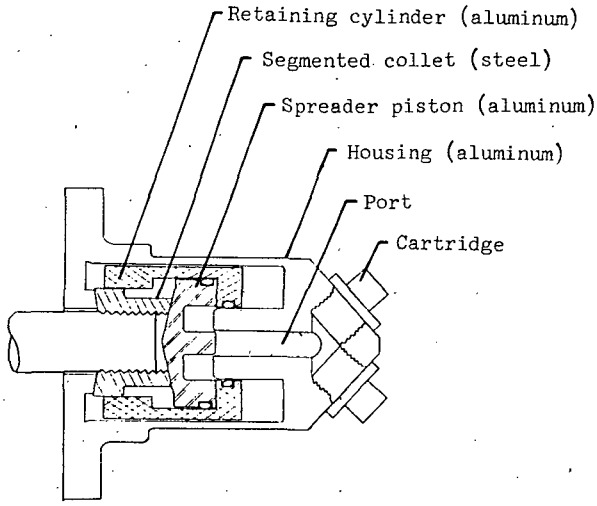

Figure 6.- Cross section of Low-Shock Design 2.

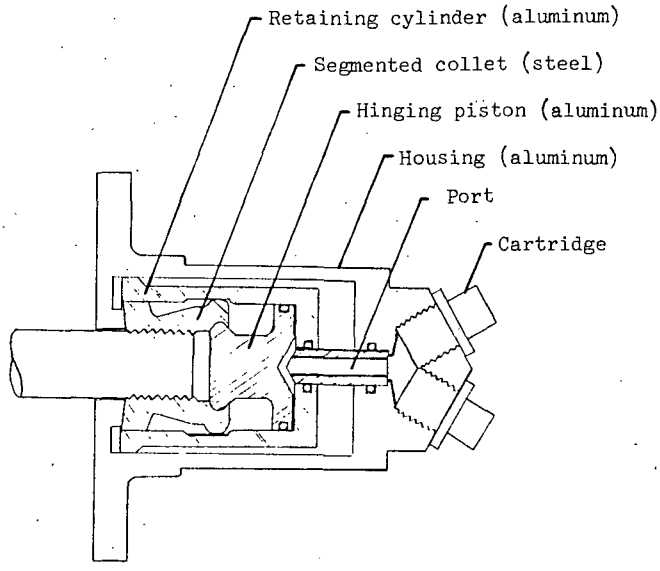

Figure 7.- Cross section of Low-Shock Design 3.

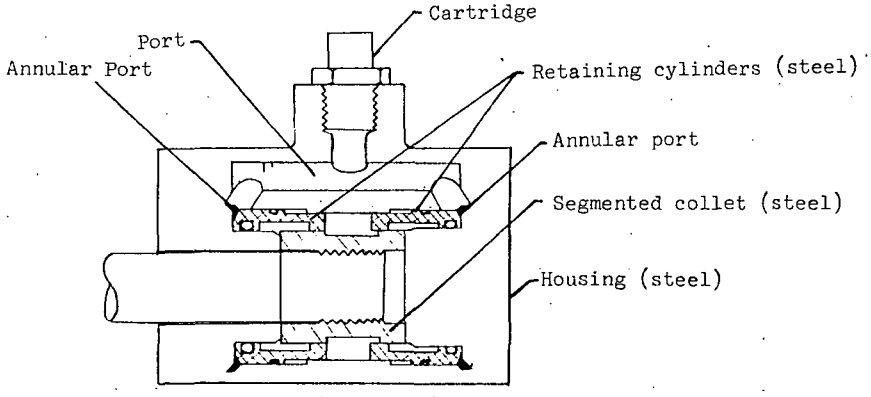

Figure 8.- Cross section of Low-Shock Design 4.

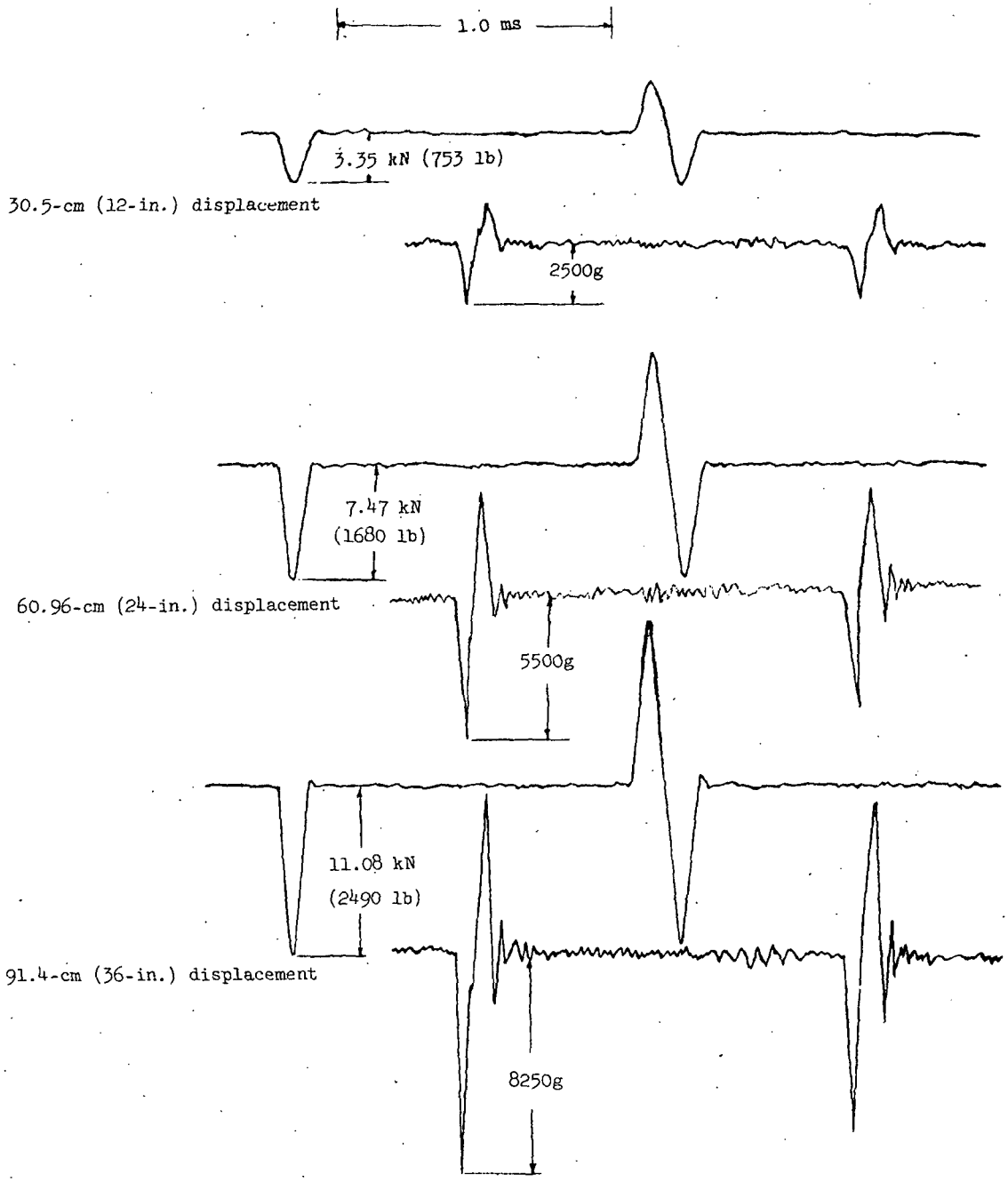

Figure 9.- Force and acceleration performance of 3.18-cm (1.25-in.) steel ball; impacts at horizontal displacements indicated. (1g = 9.807 m/sec^2.)

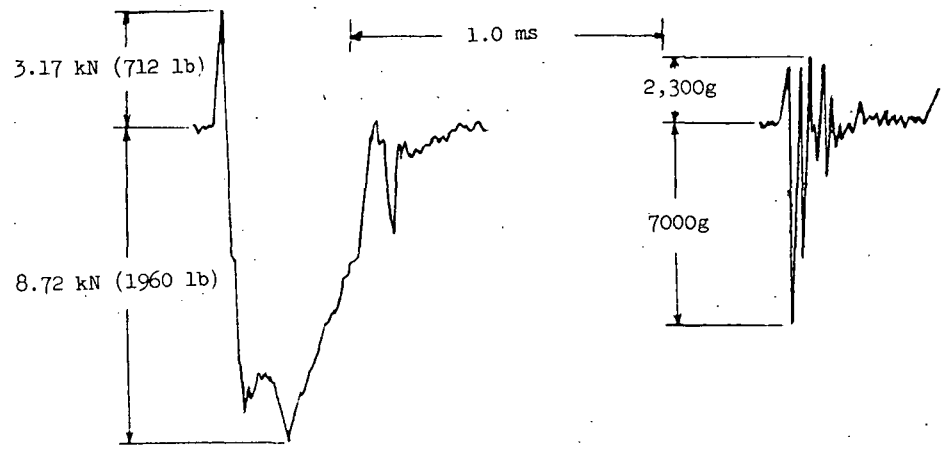

Figure 10.- Force and acceleration performance of noncaptive nut.

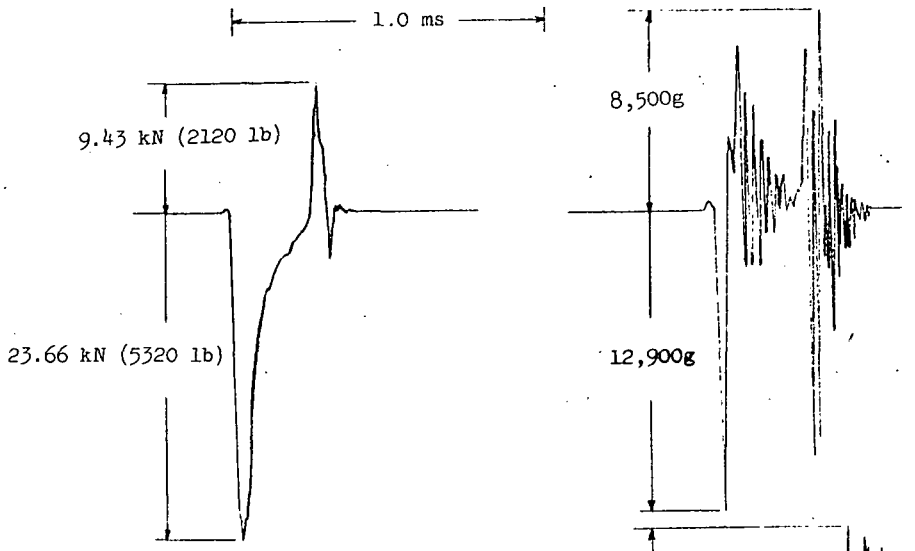

(a) Stud – force, acceleration.

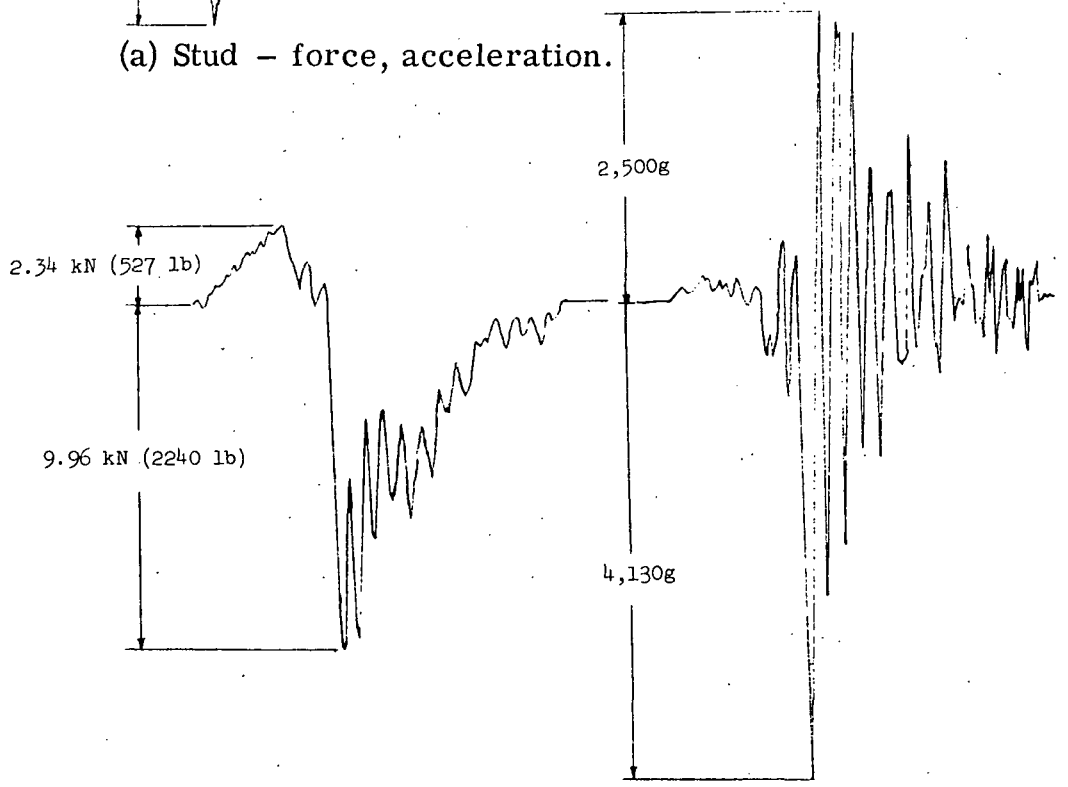

(b) Housing – force, acceleration.

Figure 11.- Force and acceleration performance of Standard Design 1.

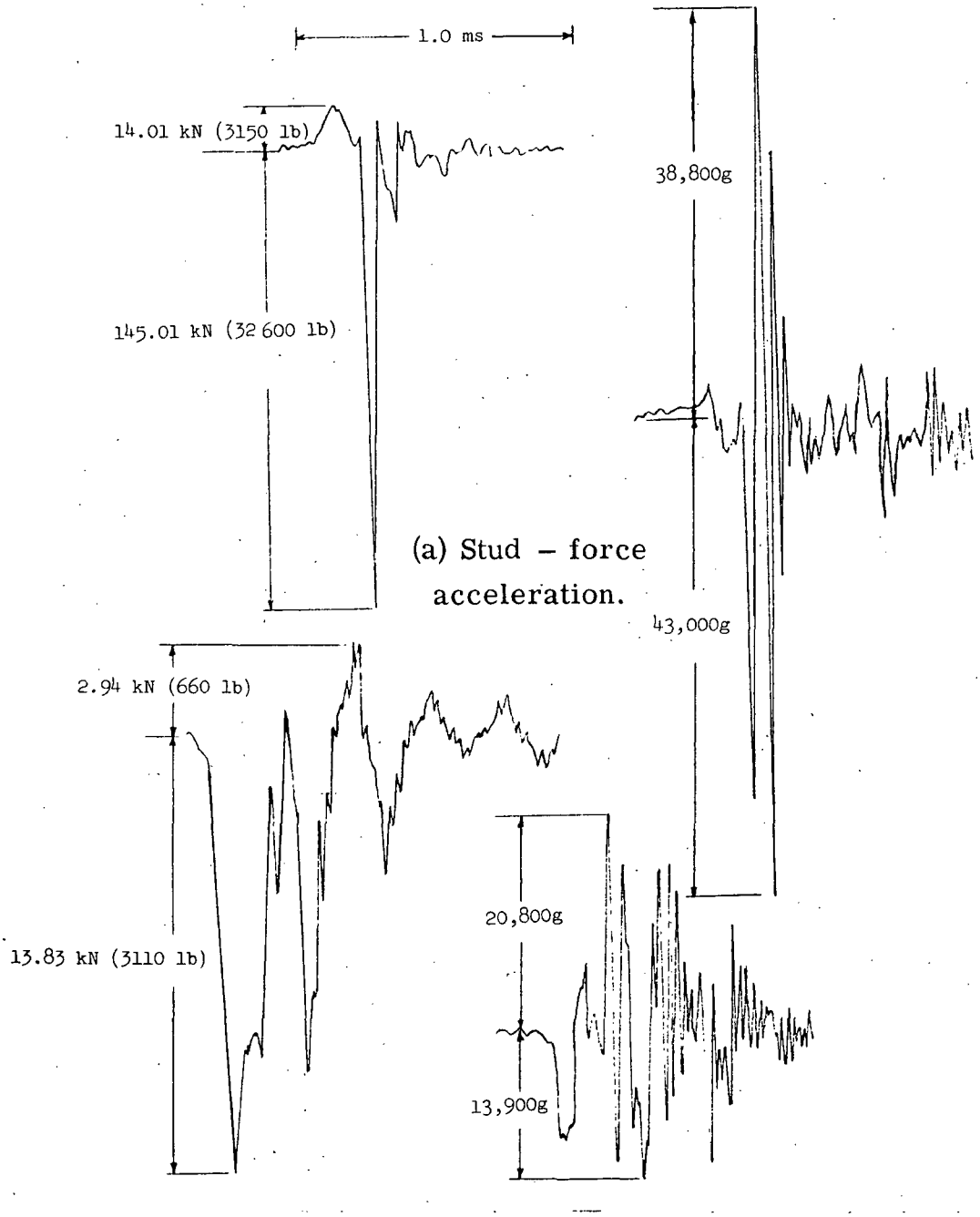

(a) Stud – force acceleration.

(b) Housing – force, acceleration.

Figure 12.- Force and acceleration performance of Standard Design 2.

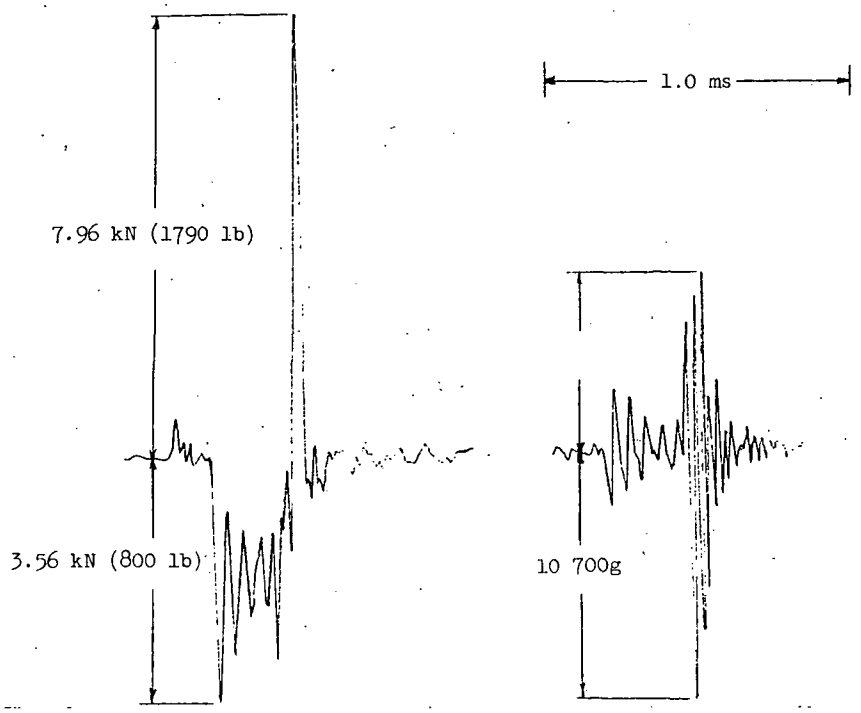

(a) Stud – force, acceleration.

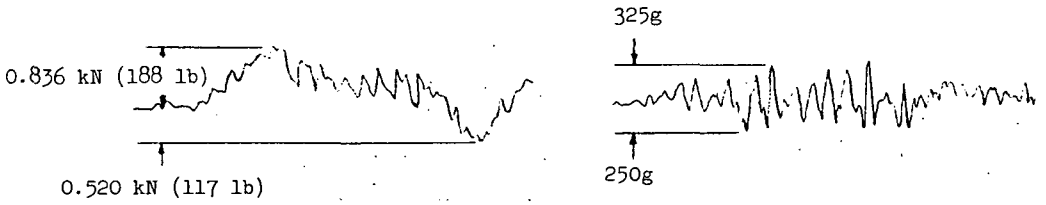

(b) Housing – force, acceleration.

Figure 13.- Force and acceleration performance of Low-Shock Design 1.

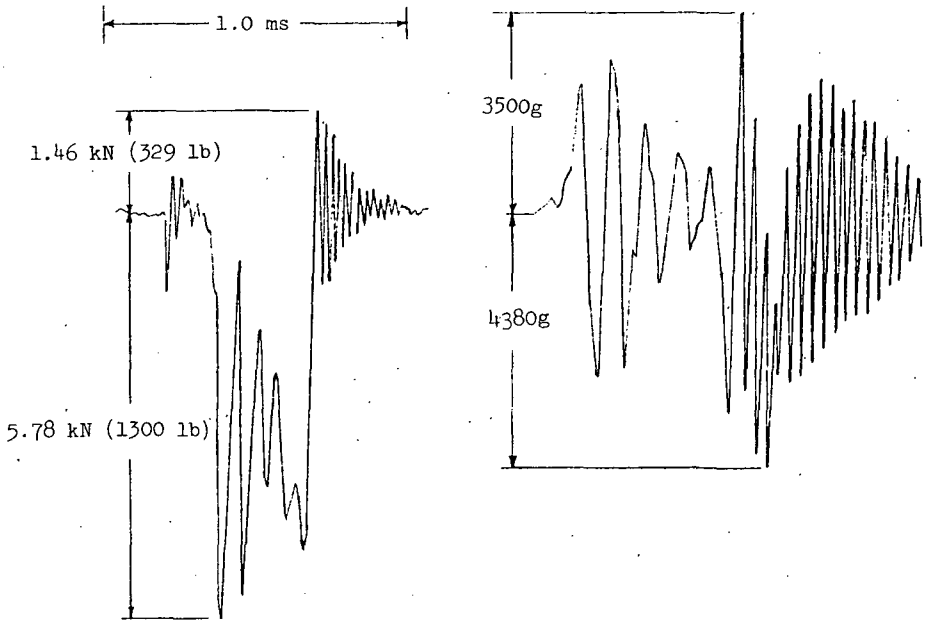

(a) Stud – force, acceleration.

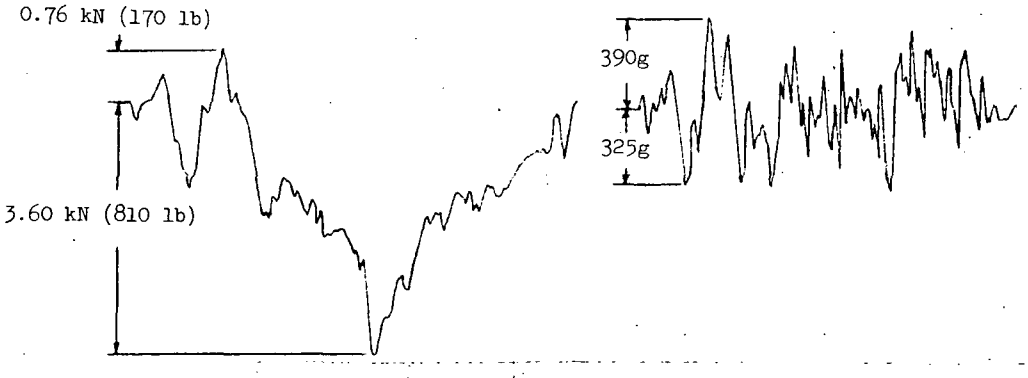

(b) Housing – force, acceleration.

Figure 14.- Force and acceleration performance of Low-Shock Design 2.

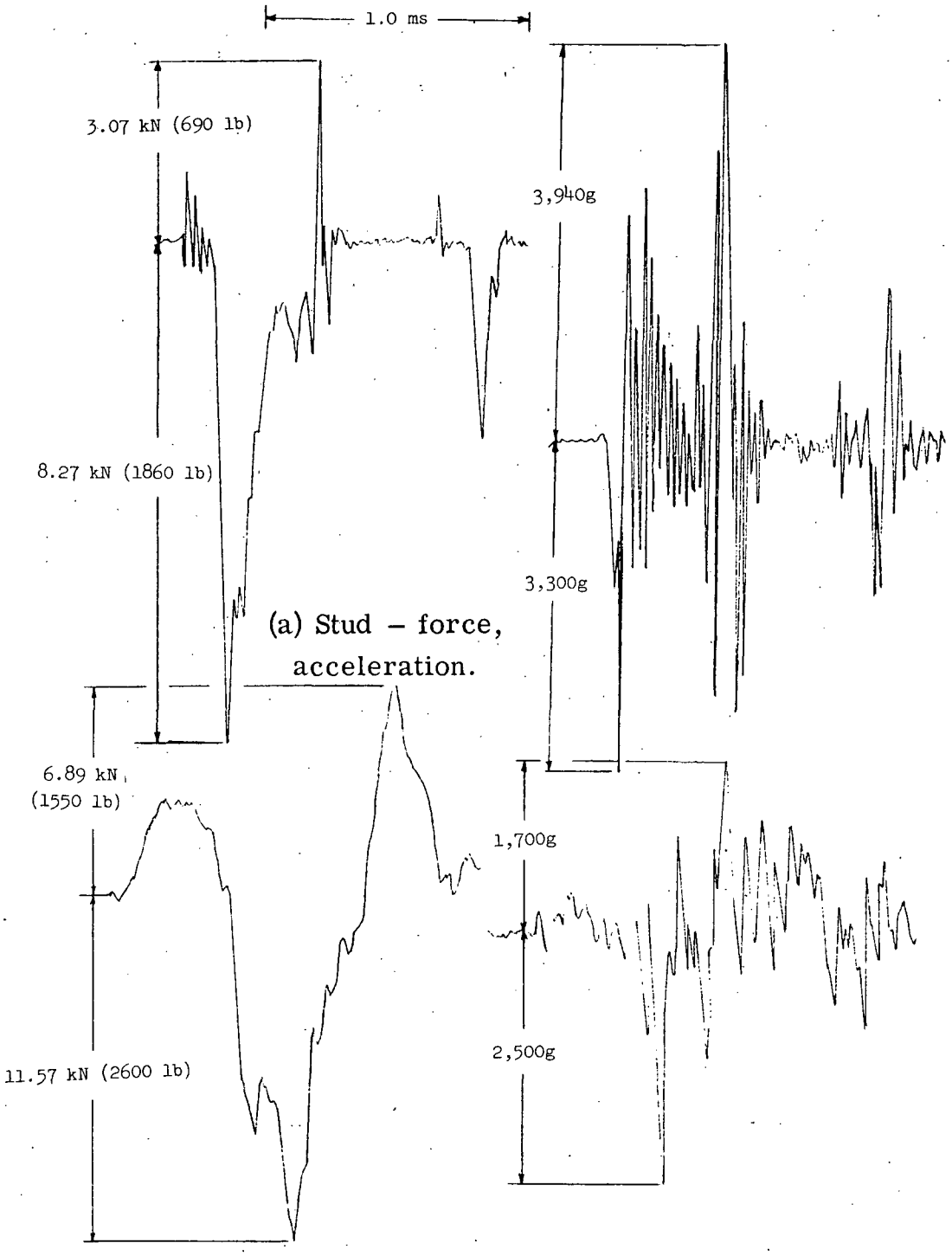

(b) Housing – force, acceleration.

Figure 15.- Force and acceleration performance of Low-Shock Design 3.

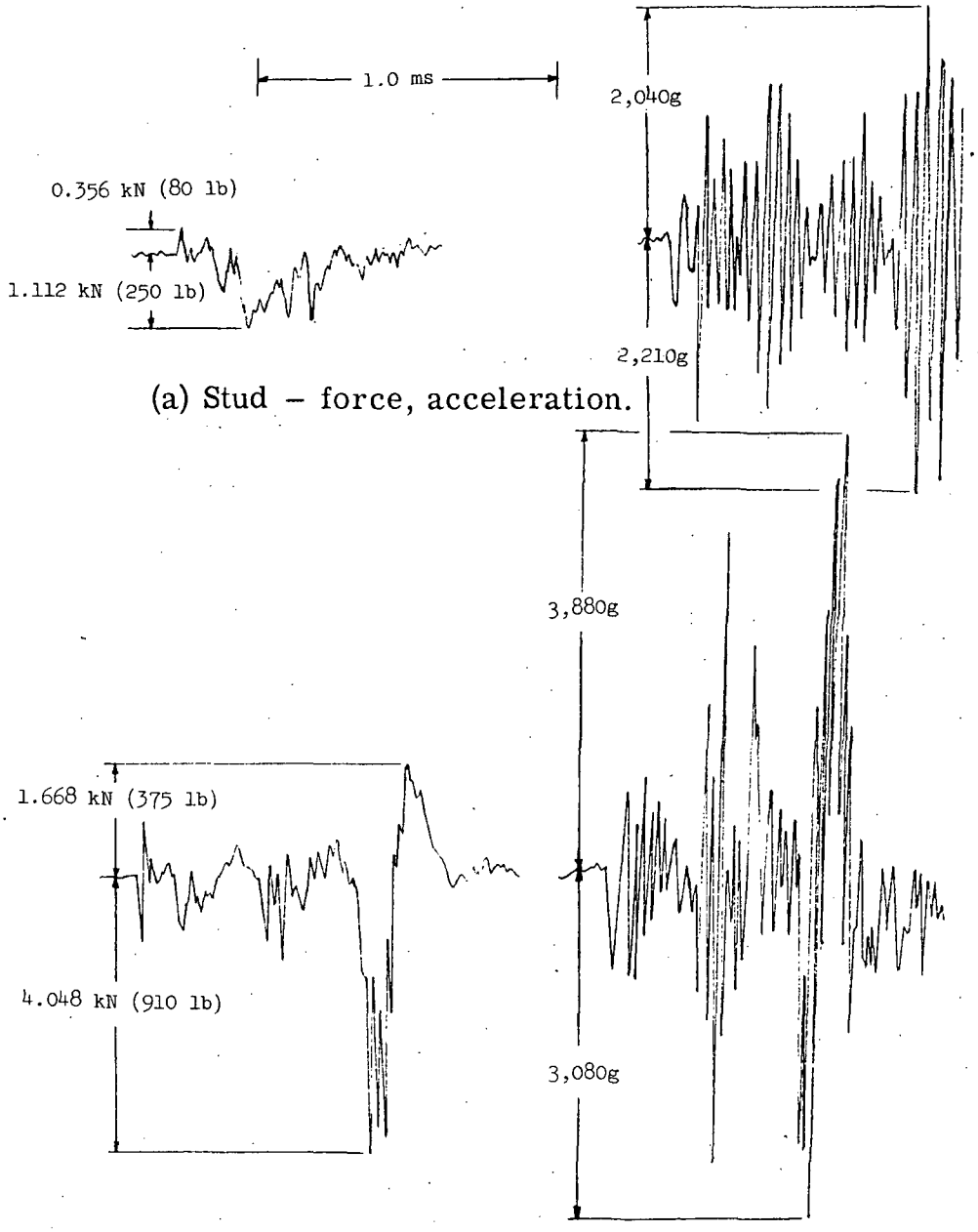

(a) Stud – force, acceleration.

(b) Housing – force, acceleration.

Figure 16.- Force and acceleration performance of Low-Shock Design 4.

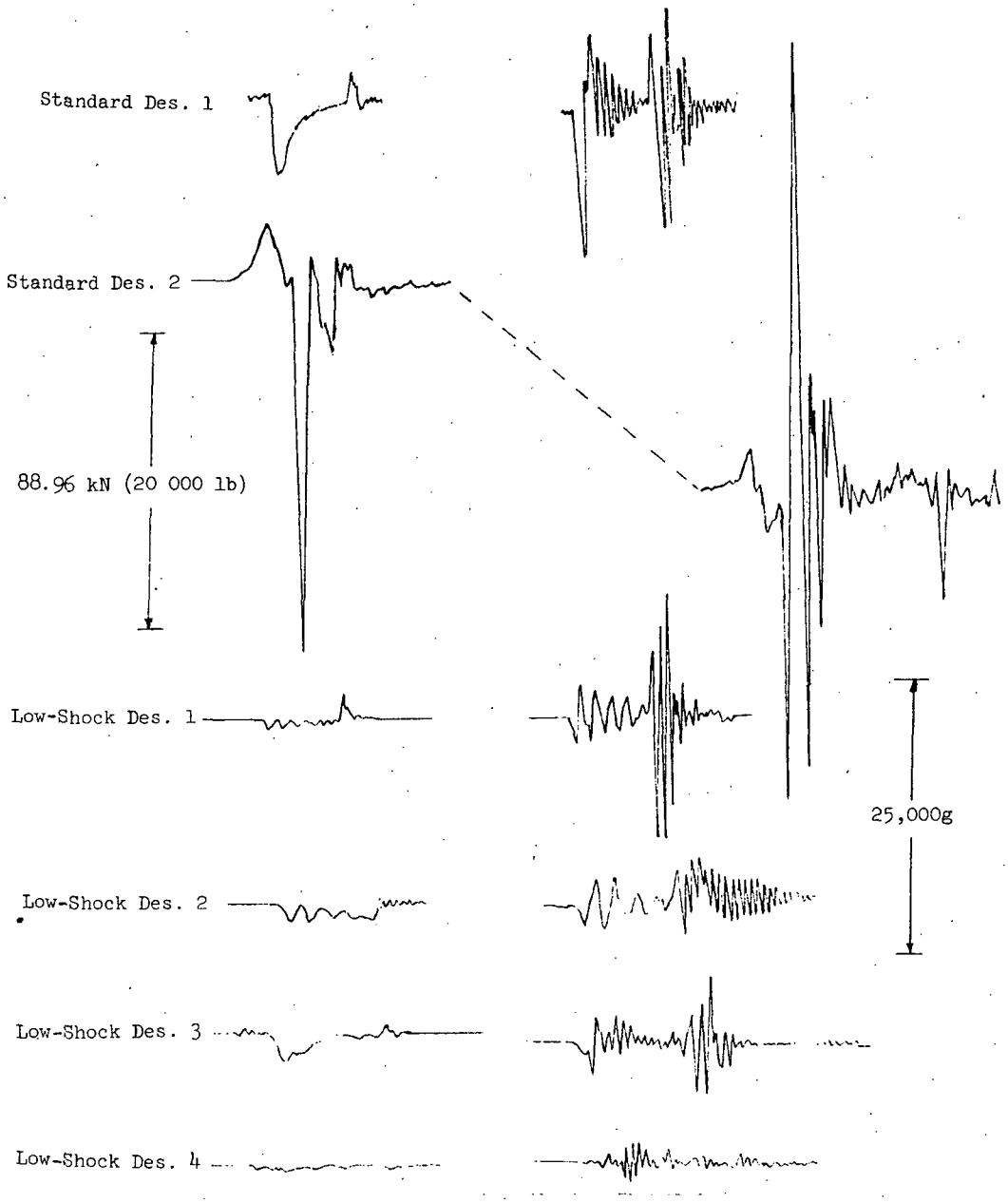

Figure 17.- Stud force and acceleration performance comparison of six separation nuts.

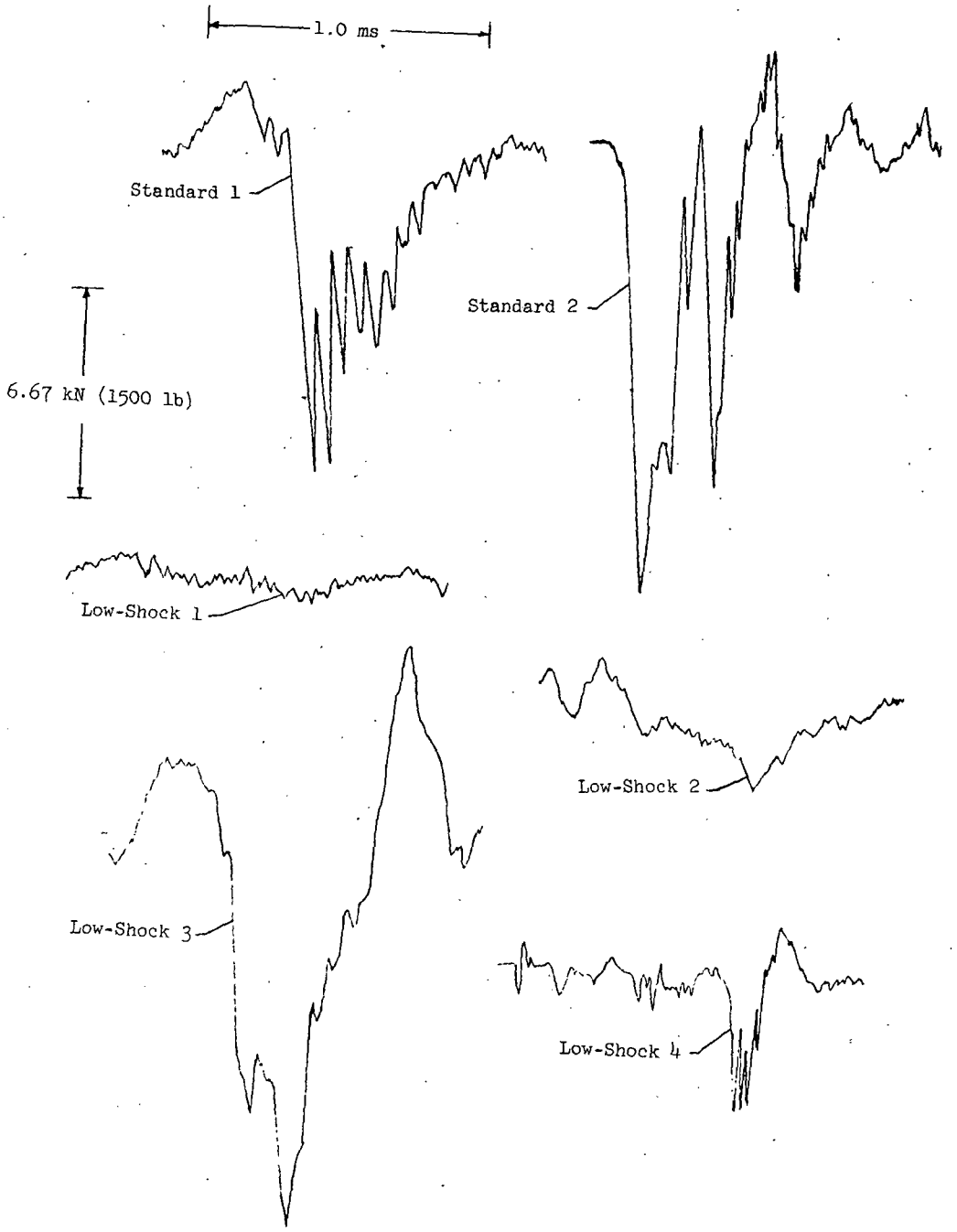

Figure 18.- Housing force comparison of six separation nuts.

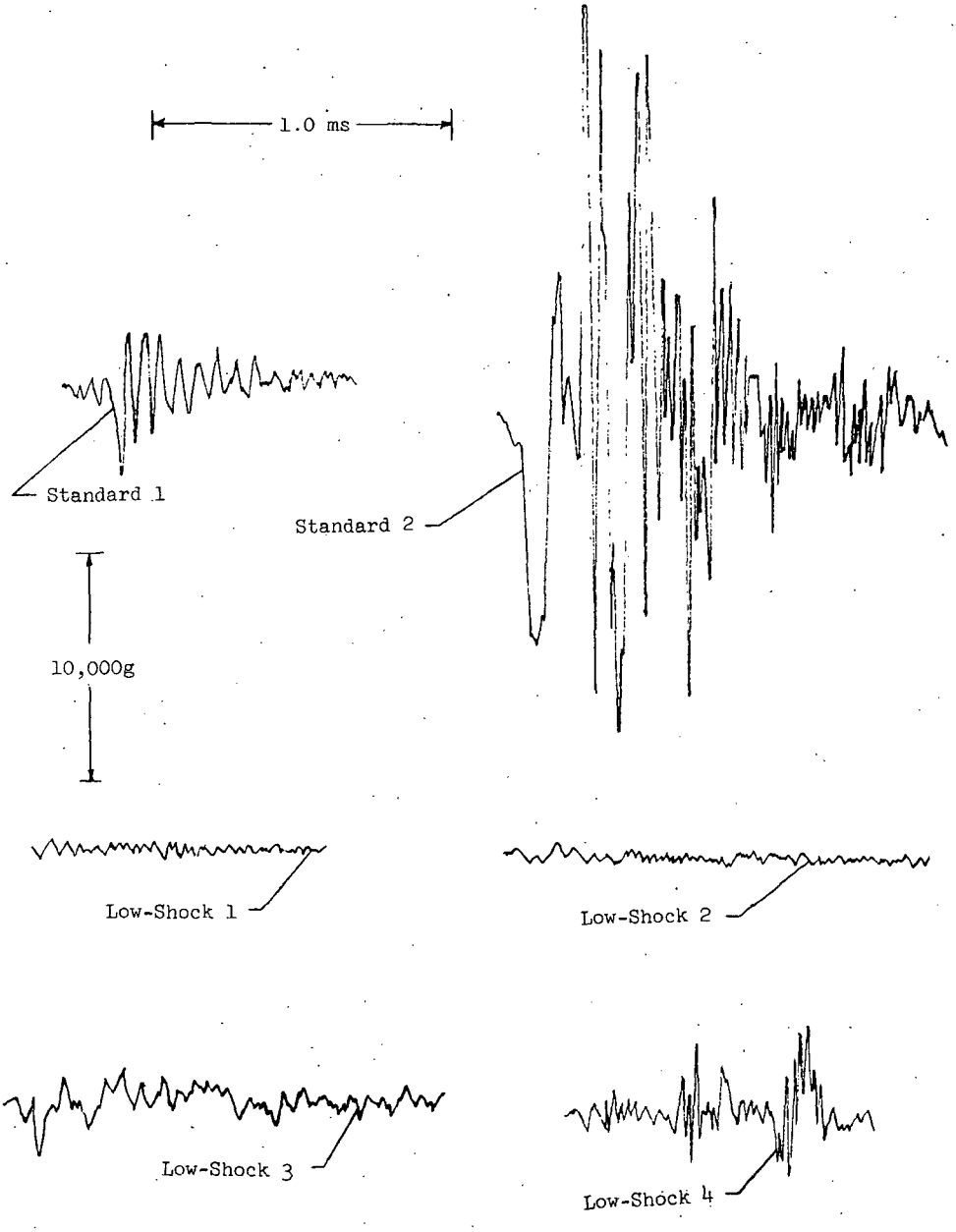

Figure 19.- Housing acceleration comparison of six separation nuts.

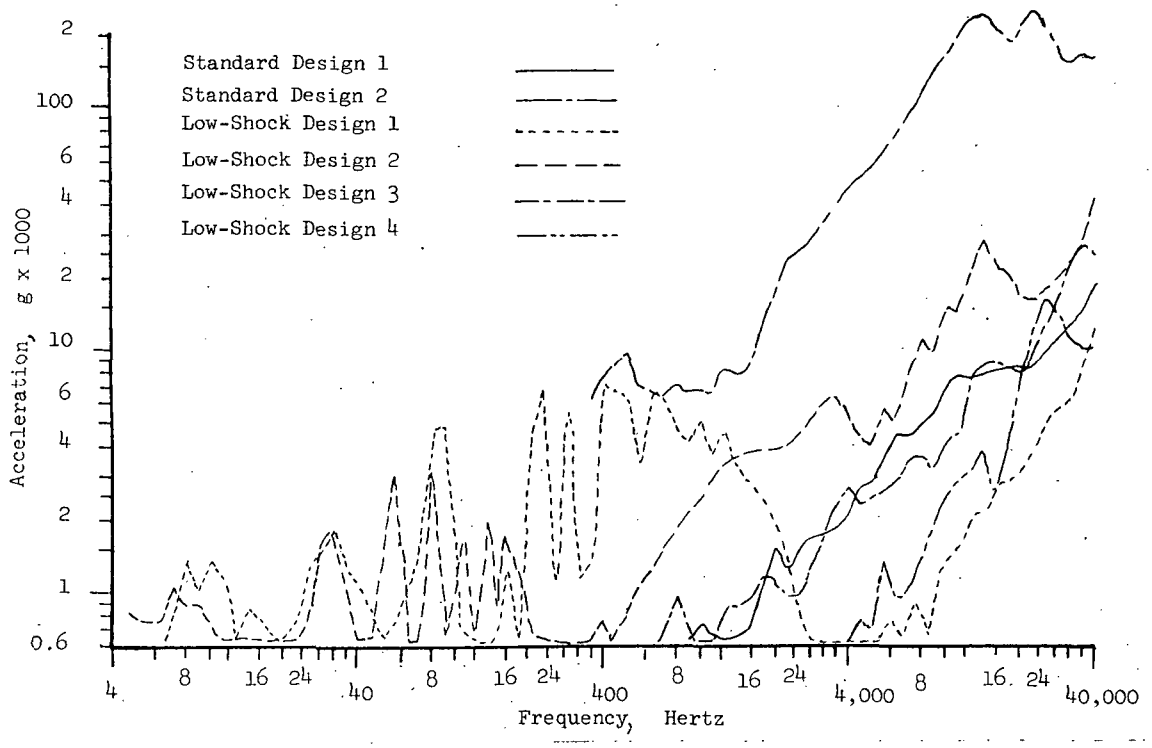

Figure 20.- Stud performance spectra comparison.

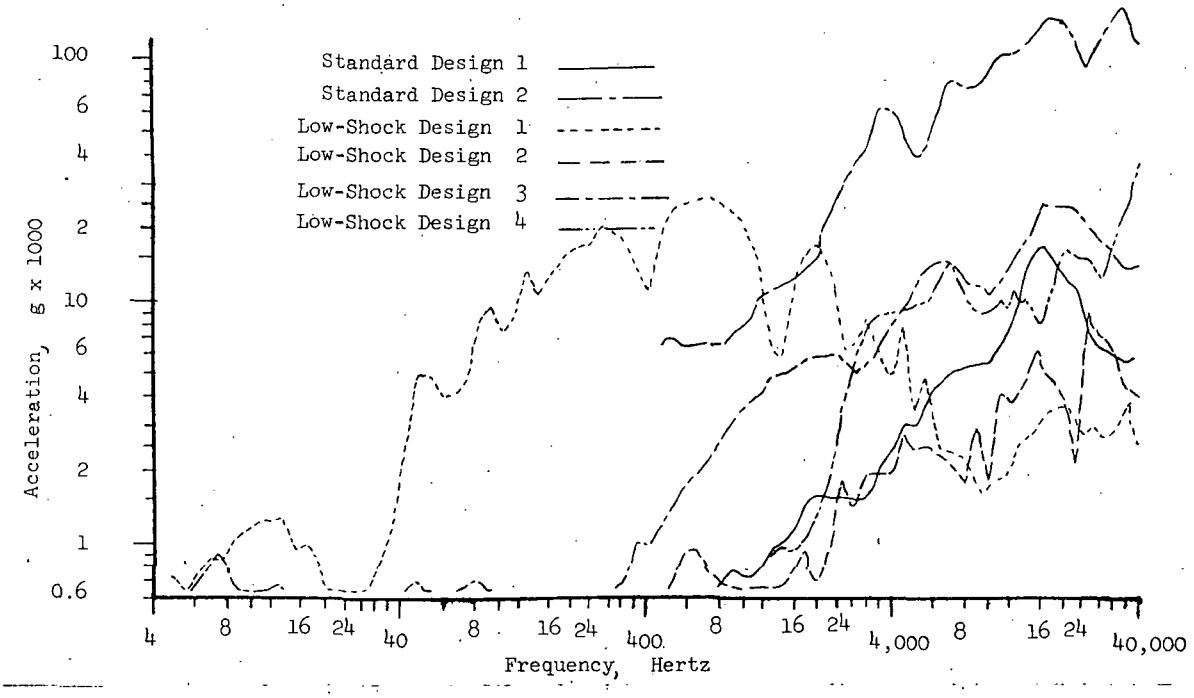

Figure 21.- Housing performance spectra.

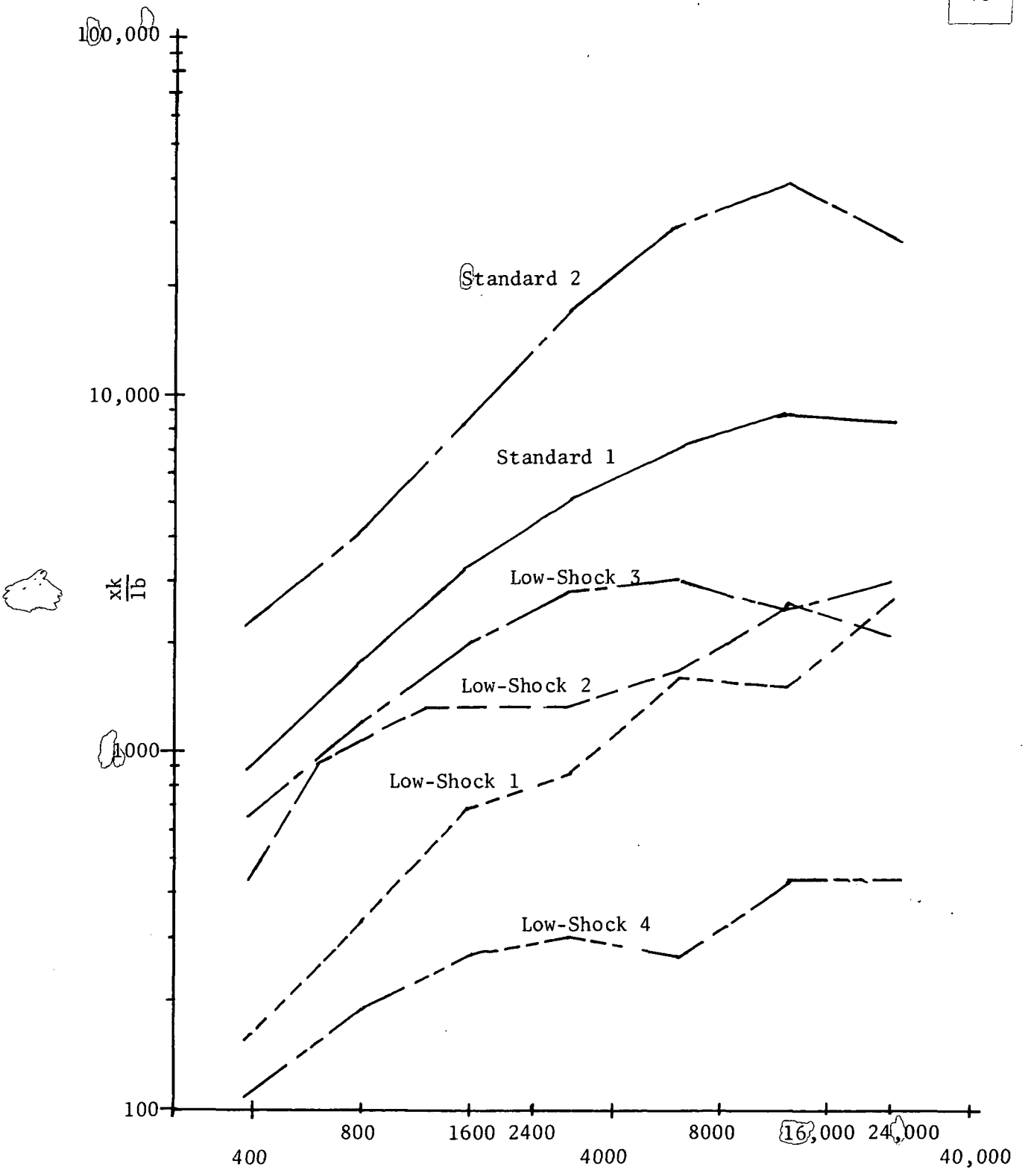

Figure 22 - Calculated displacement shock spectra for stud force

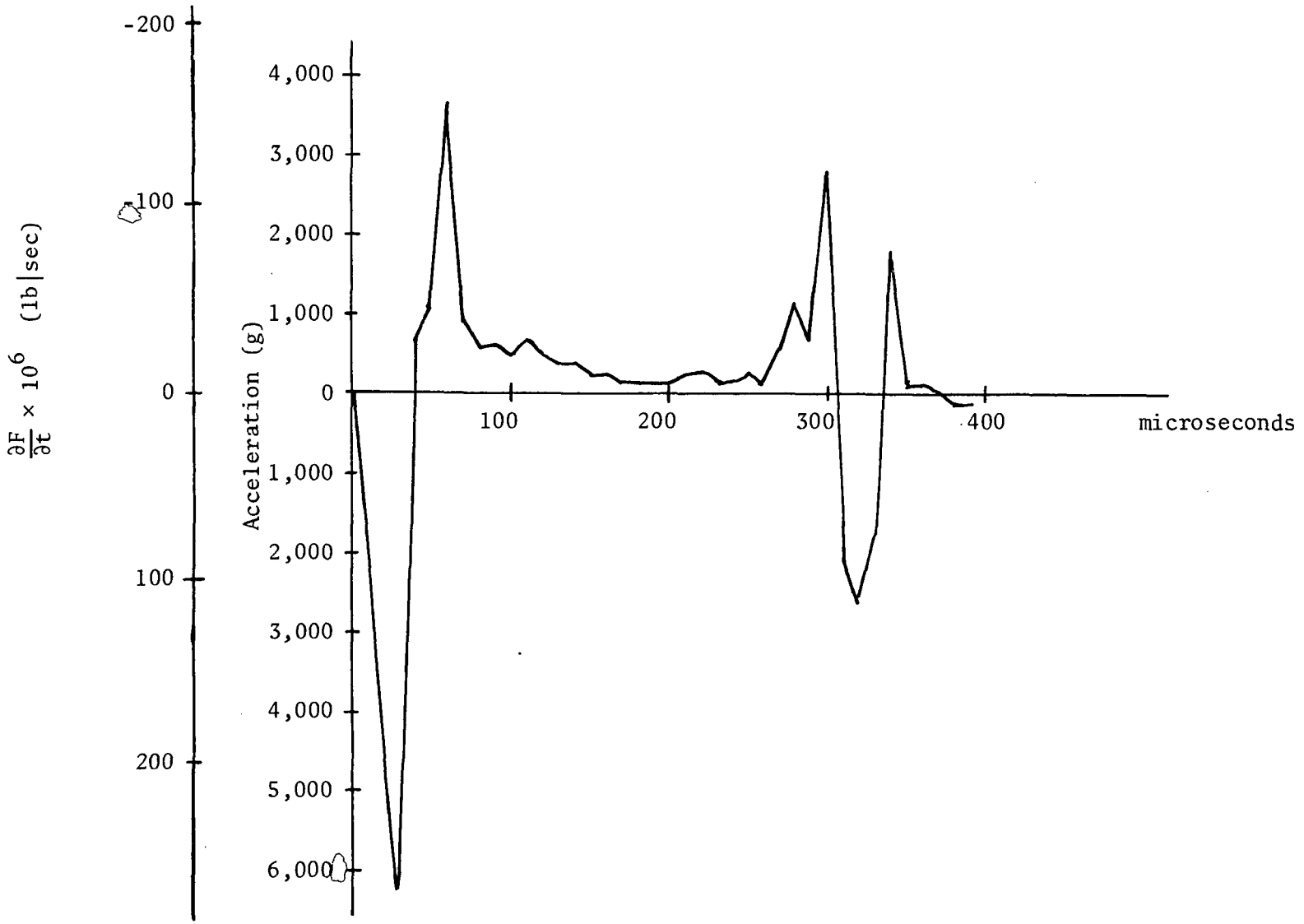

Figure 23 - Calculated $\frac{\partial F}{\partial t}$ and acceleration for Standard Design 1

Standard Design I

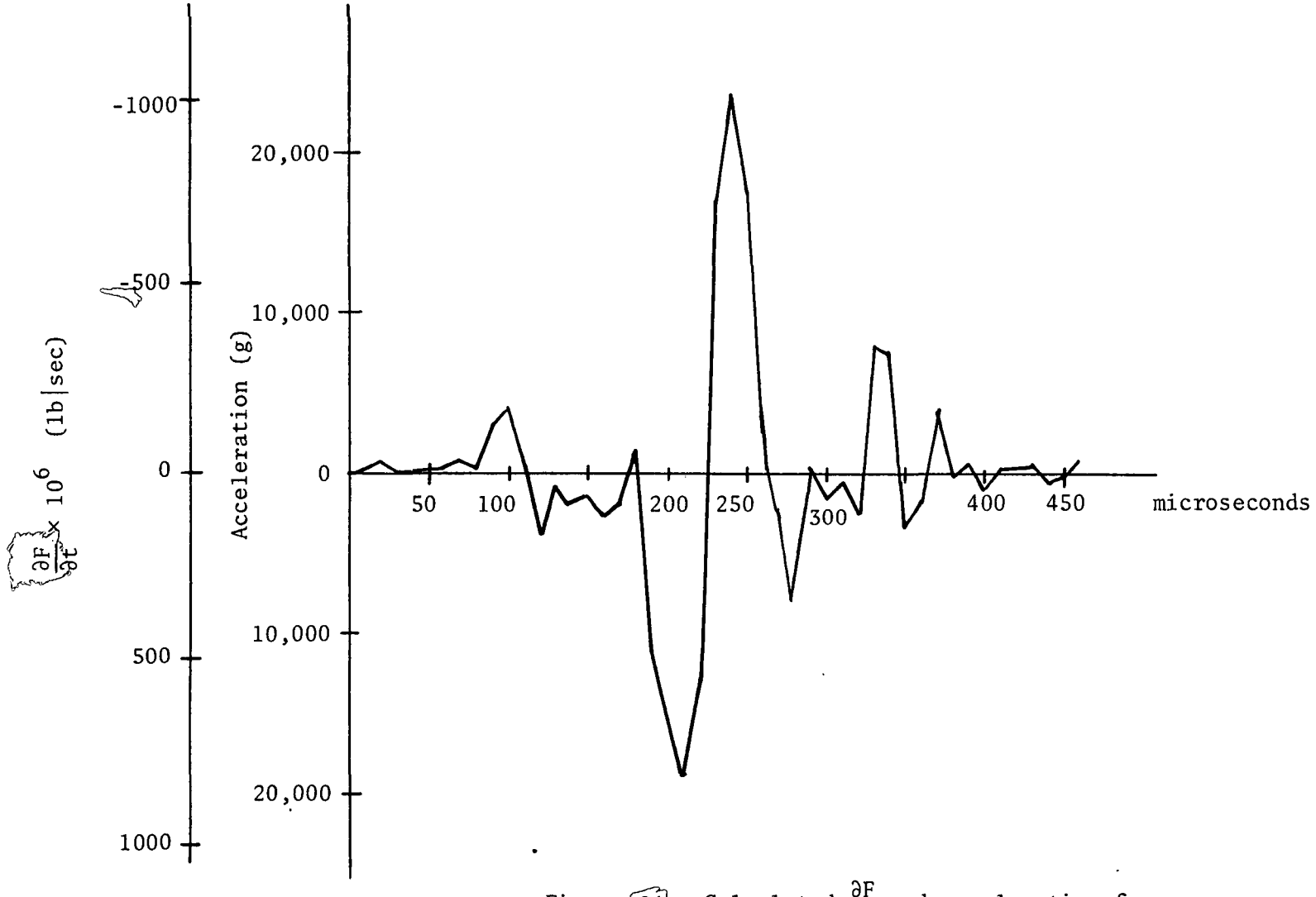

Figure 24 - Calculated $\frac{\partial F}{\partial t}$ and acceleration for Standard Design 2

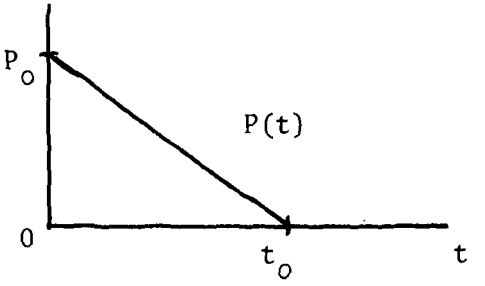

Timewise loading

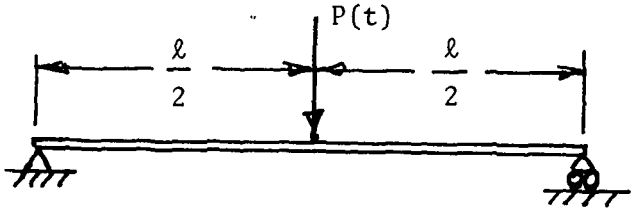

Hinged-hinged beam

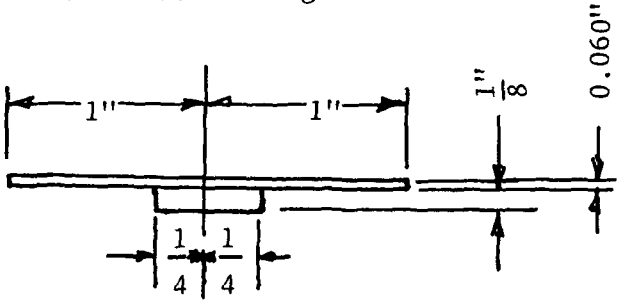

Beam cross-section

Figure 25 - Theoretical beam under impulsive loading

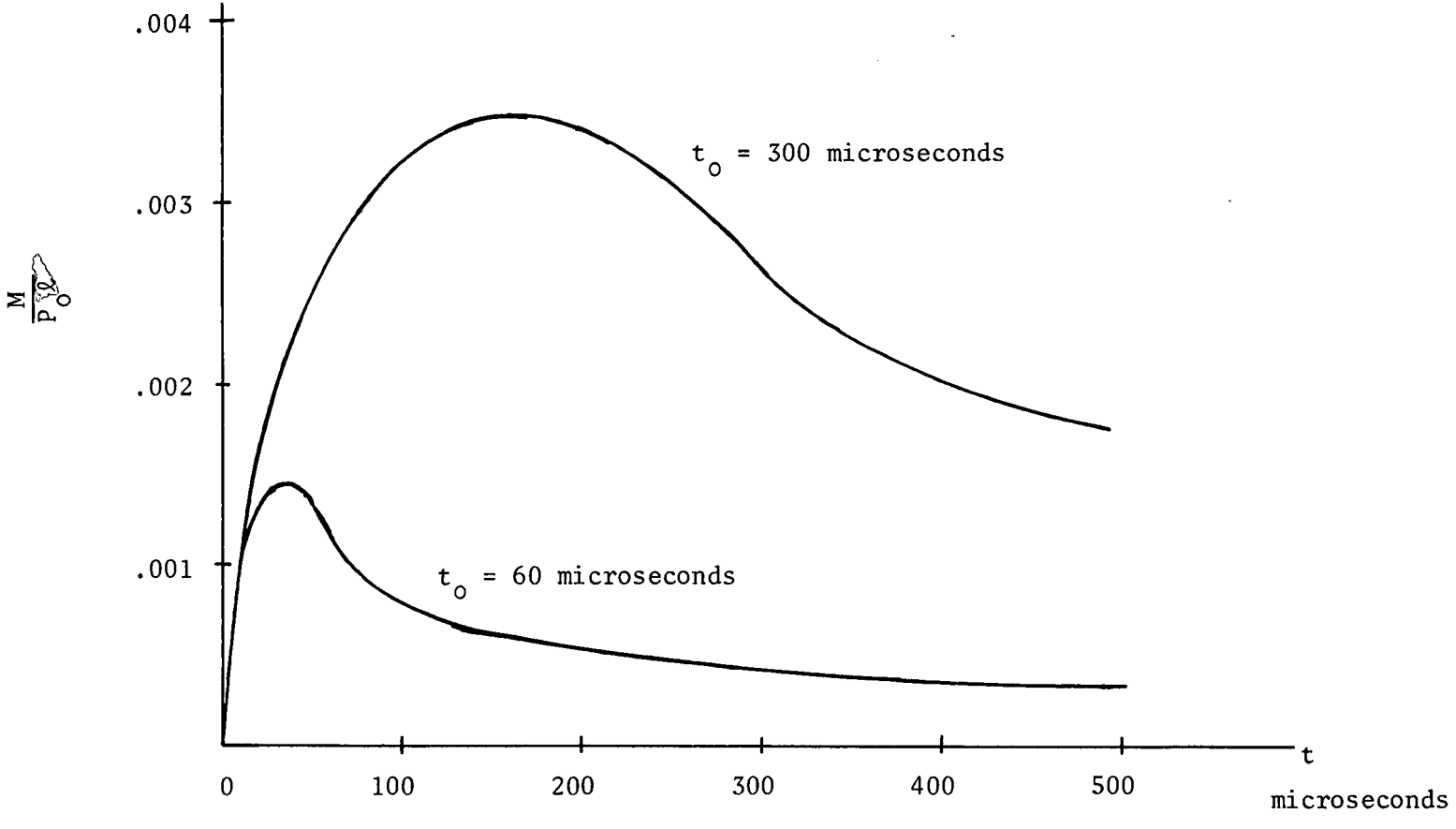

Figure 26 Calculated moment at center of hinged-hinged beam under impulsive loading

APPENDIX A

THEORETICAL BEHAVIOR OF THE SENSING BAR

Ideal Axial Behavior of the Thin Bar

The long, thin bar has been used in experiments for measurements of high pressures for some time, and is commonly called the Hopkinson pressure bar. In the ideal case, if the wave length of the pressure pulse is at least ten times the bar diameter, the bar behaves according to the wave equation in one dimension, which is

$$\frac{\partial^2 u(x,t)}{\partial t^2} = a^2 \frac{\partial^2 u(x,t)}{\partial x^2} \qquad \text{(A-1)}$$

Here $u(x,t)$ is the particle displacement at a distance x from the end of the bar. Also, $a = (E|\rho)^{1/2}$ is the speed of sound in the elastic bar, with E the Young's Modulus and ρ the mass density of the material.

The travelling wave solution is of the form

$$u = g(c_1 + x - at) + f(c_2 + x + at) \qquad \text{(A-2)}$$

The first term indicates a wave travelling in the positive x direction (or to the right); the second term, a wave to the left. The constants c_1 and c_2 can be chosen to position the wave at $t = 0$. Theoretically the wave retains the same shape as it travels along the bar.

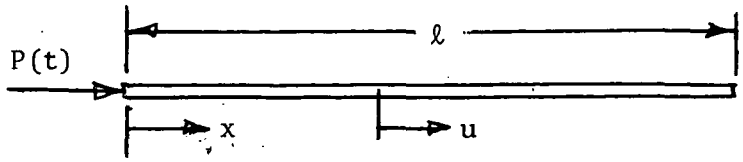

Fig. A-1 Hopkinson Pressure Bar

For a wave to the right, the strain ε would be

$$\varepsilon = \frac{\partial u}{\partial x} = g'(c_1 + x - at) \tag{A-3}$$

and the stress σ is

$$\sigma = E\frac{\partial u}{\partial x} \tag{A-4}$$

It is assumed that if the bar is cut perpendicular to its axis, the stress would be uniformly distributed over the area A of the cross-section, so the total force F at a point x would be

$$F = AE\frac{\partial u}{\partial x} \tag{A-5}$$

At the free end, where $x = \ell$, the force $F = 0$, and it can be shown that the particle velocity $\frac{\partial u}{\partial t}(\ell,t)$ and acceleration $\frac{\partial^2 u}{\partial t^2}(\ell,t)$ will be twice what it was in the wave before reaching the end. If the wave approaching a free end is compressed, it will be reflected as a tensile wave.

The particle velocity and the acceleration for a wave to the right will be

$$\frac{\partial u}{\partial t} = -ag'(c_1 + x - at) \tag{A-6}$$

$$\text{and } \frac{\partial^2 u}{\partial t^2} = a^2 g''(c_1 + x - at) \tag{A-7}$$

Here the prime denotes the derivative of the function. If we differentiate (A-3) with respect to time

$$\frac{\partial \varepsilon}{\partial t} = \frac{\partial^2 u}{\partial x \partial t} = -ag''(c_1 + x - at) \tag{A-8}$$

eliminating g'' from (A-7) and (A-8) gives

$$\frac{\partial^2 u}{\partial t^2}(x,t) = -a\frac{\partial \varepsilon(x,t)}{\partial t} \tag{A-9}$$

Thus the shape of the strain-time curve at a point may be obtained by integrating the acceleration-time record, measured at the same point. In the apparatus used, the acceleration was measured at the free end of the bar, while the strain was measured at distances of 10 and 20 inches from the other, loaded end. The acceleration at the free end, at $x = \ell$, is twice what it would be at the strain gauge, so

$$\frac{\partial \varepsilon}{\partial t}\left(x = \frac{20}{144}\,\ell, t\right) = -\frac{1}{2a} \cdot \frac{\partial^2 u}{\partial t^2}(\ell, t) \qquad \text{(A-10)}$$

Since the bar was 144 inches long, the 20-inch station is at $x = \frac{20\ell}{144}$.

After the detonation of the nut, the stress wave will be initiated which will travel the length of the bar and return as a reflected wave. If the bar is 144 inches long, and the strain gauge is 20 inches from the loaded end, the front of the wave will travel

$$2(144 - 20) = 248 \text{ inches}$$

before a reflected wave front reaches the strain gauge. The wave velocity $a = 200{,}000$ in./sec. so the usable portion of record, before a reflected wave is superimposed, is

$$248/a = 1.24 \times 10^{-3} \text{ seconds}$$

Departures from Ideal Axial Behavior

The following factors will cause departures from the ideal behavior noted above:

1. The load is not applied uniformly over the bar area, A, by the nut. Thus the wave must travel some distance before it "settles down" to a plane wave. Experiments with mechanical impact and explosive bolts tended to indicate that ten diameters should be sufficient distance for the wave to settle down.

2. The load, P(t), may be applied eccentrically by the nut. This will cause bending strains to be superimposed on the axial strains.

The problem is solved by locating the strain gauges diametrically opposite each other at a particular bar station. Bending strains are then eliminated from the record by wiring the two gauges in series, or by connecting them to opposite arms of the bridge.

3. The load may be so great that the bar material is loaded into the inelastic range. Equation (A-1) does not apply, and the wave will be modified in magnitude and shape as it travels along the bar. This can be corrected by increasing the bar diameter, or, better yet, by using higher strength materials.

4. The length of the pulse may be so short, or its frequency content so high, that the associated wave lengths are less than ten times the bar diameter. Again Equation (A-1) will not apply. Two-dimensional effects in the bar must be considered, and the wave will disperse, or change shape, as it travels along the bar. This was discussed in detail in Reference [2], because the problem arose in testing explosive bolts, where the pulse length was only 12 micro-seconds long. One solution would be to decrease the bar diameter, but this results in increased stresses.

Calibration of the Apparatus

In order to calibrate the apparatus, hardened steel spheres of various diameters were impacted against the end of the bar. The impact of a sphere on a bar of constant diameter is well understood. The tests were done primarily to determine the effect on the wave shape of adaptors used to accommodate the explosive nuts.

The steel spheres were supported like a simple pendulum, of length s, on the end of piano wire. The pull-back p varied from 12 to 36 inches. Then $\sin\theta = p/s$ and the height h the sphere was raised was $h = s(1 - \cos\theta)$.

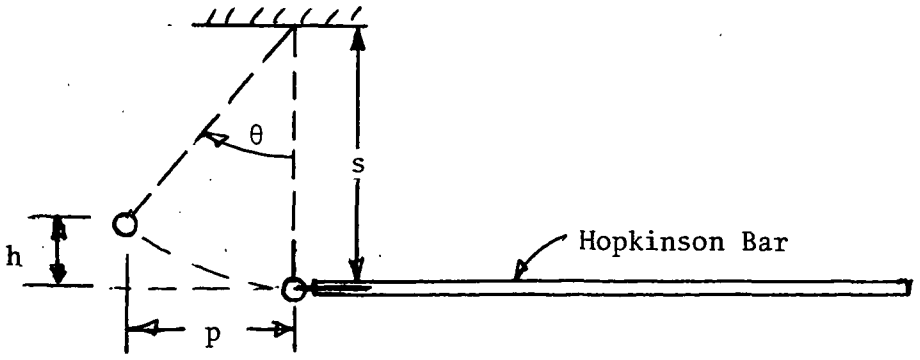

Figure A-2 Calibration with Spheres

The velocity of the sphere on impact would be about $\sqrt{2gh}$, where g is the acceleration due to gravity.

The theory of impact between two elastic spheres is outlined in Reference [3], based on the Hertz contact theory. The contact time and contact force versus time are predicted knowing the dimensions, material properties of the spheres, and their relative velocity upon impact. For a sphere striking a rod, the results do not strictly apply, but it has been found that if the rod is taken as a sphere of very large radius, the contact time can be predicted accurately. For a 1-1/4 inch diameter steel sphere striking the steel bar, the contact time is predicted to be 120×10^{-6} seconds, which is very close to the experimental value. The equation (A-10) is also readily verified by experiment, that is, that the acceleration is proportional to the slope of the strain-time curve. If, for example,

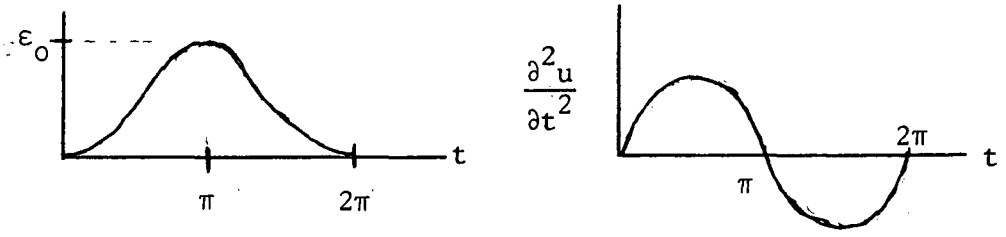

Fig. A-3 Strain-acceleration Relationship

the $\varepsilon = \frac{\varepsilon_o(1 - \cos\omega_n t)}{2}$ then

$$\frac{\partial^2 u}{\partial t^2} = \frac{-a\varepsilon_o \omega_n \sin\omega_n t}{2}$$

Although these are not the exact mathematical shapes, the relationship (A-10) is confirmed in the experimental data. Since the strain is the integral of the acceleration, it is easier to measure, with regard to high frequency content, than the acceleration.

In addition to plain bar ends, several nut adaptors were attached to the bar end for evaluation. An adaptor was chosen which had little effect on the pulse shape. As expected, it was the shortest, least massive adaptor.

Bending Strain in the Measuring Bar

If the loading were applied axially to the end of the bar, there would be no bending. However, the data indicate appreciable bending in some cases, which means the nuts produce some eccentricity in the loading, causing a bending moment as well as an axial force to be applied.

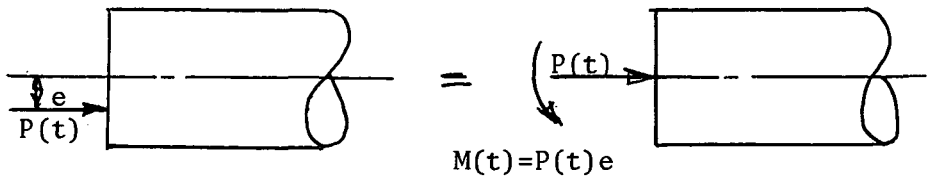

Fig. A-4 Bending Due to Eccentric Axial Force

Another possibility, which seems less likely, is that $P_1(t)$ is applied at an angle, resulting in an axial force and a lateral shear force V(t).

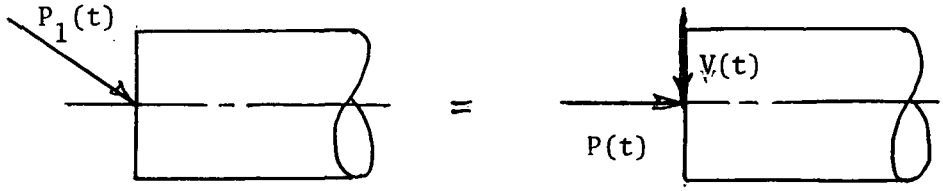

Fig. A-5 Loading Producing Lateral Shear Force

A bending pulse always disperses as it travels down the bar, which means it changes magnitude and shape.

Parker [4] has shown that if a half-sine pulse bending moment of magnitude 71 in. lb. and duration of 14 microseconds were applied to a bar of 0.516 inches diameter, the bending pulse would attenuate to 50 in. lb. by the time it travelled two diameters from the end, and to about -30 in. lb. peak at 16 diameters from the end. On another example using a one-inch diameter bar, a half-sine lateral shear load V(t) of 30,000 pound magnitude, and a 10 microsecond duration, a peak bending moment of 6,000 in. lb. at a station 10 inches from the bar end is produced.

Jent [5] applied an axial pulse of 200 microseconds duration and known eccentricity e to a 3/4 inch diamater steel bar. For 3/16 inch eccentricity, he found that the peak bending strain was about equal to the peak axial strain.

For the present experiment, bending strain ε_B

$$\varepsilon_B = \frac{Mr}{EI} \quad \text{or} \quad \varepsilon_B = \frac{Per}{EI}$$

if M = Pe. The axial strain ε_A is

$$\varepsilon_A = \frac{P}{AE}$$

Then, if there is no attenuation of the bending wave,

$$\frac{\varepsilon_B}{\varepsilon_A} = \frac{erA}{I}$$

Since $I = \frac{Ar^2}{4}$

$$\frac{\varepsilon_B}{\varepsilon_A} = \frac{4e}{r}$$

then $\varepsilon_B = \varepsilon_A$ if $e = \frac{r}{4}$, so an eccentricity of only 1/8 inch could lead to bending strains of the same magnitude as the axial strain. This is important and indicates that in a timewise analysis of a structure, using the applied loads measured from the nuts, a moment as well as an axial force should be applied. To determine the moment-time loading from each bolt, analysis would need to be performed of the bar vibrating laterally as a beam, as in Reference [4], to account for attenuation of dispersion.

Shock Spectrum Versus Timewise Loading for Analysis

It has been common to process acceleration data to obtain a shock spectrum. This indicates the peak response of a single-degree-of-freedom-system, but does not retain phase information or the time at which the peak occurs. Then, in a normal mode analysis of a structure, peak response can be calculated, from the shock spectrum, for each mode. However, the means of combining peak modal responses is lost. If a timewise loading is known, the modal responses can be added correctly at each instant of time. This is especially important if many modes are excited, as in a spacecraft.

APPENDIX B

SHOCK SPECTRUM

The shock spectrum is the plot of peak response of a single-degree-of-freedom system versus the natural frequency ω_n of the system. The input may be a base motion z(t), as shown in Figure B-1, or a force P(t), as shown in Figure B-2.

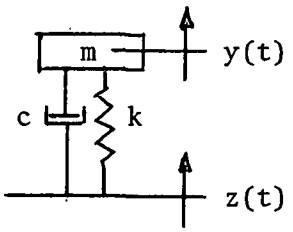

Figure B-1

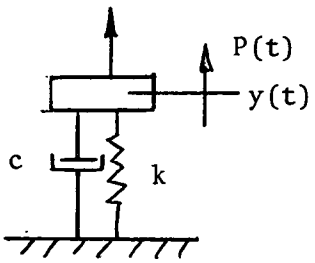

Figure B-2

The equation of motion for the system with base motion is

$$m\ddot{y} + c(\dot{y}-\dot{z}) + k(y-z) = 0 \qquad \text{(B-1)}$$

Here y and z are absolute displacements. Also, $\omega_n^2 = k|m$. If (B-1) is written using $x = y-z$, the result is

$$m\ddot{x} + c\dot{x} + kx = -m\ddot{z}(t) \qquad \text{(B-2)}$$

For the force input system, the equation is

$$m\ddot{y} + c\dot{y} + ky = P(t) \qquad \text{(B-3)}$$

Note that equations (B-2) and (B-3) are similar in form but there are three essential differences between the two. In the first equation the input is base acceleration; in the second it is applied force. The sign of the right-hand side of the first is different from that of the

second; and x is relative displacement while y is absolute.

Various response quantities may be plotted versus natural frequency, that is, peak relative or absolute displacement, velocity, or acceleration. Also, sometimes pseudo-velocity is plotted which is $\omega_n y$ and is not in general equal to $\dot{y}$.

Usually the duration t_o of the shock input $\ddot{z}(t)$ or $P(t)$ is short, and the inputs are zero for $t > t_o$. However, the response continues as a free vibration for $t > t_o$. Sometimes only the maximum response is recorded during the time $0 \leq t \leq t_o$ and the corresponding plot versus ω_n is called the primary spectrum. A plot of maximum response ocurring for $t > t_o$ is called a residual spectrum and can be directly related to the Fourier spectrum. The plot of the maximum response, regardless of when it occurs, is sometimes called a maxi-max spectrum.

In reference (1), plots of primary spectra for absolute acceleration $\ddot{y}(t)$ are given for various measured accelerations $\ddot{z}(t)$. The value of damping used was five percent of critical damping c_c, where $c_c = 2m\omega_n$ and $c/c_c = \zeta$.

Equation (B-2) can be written as

$$\ddot{x} + 2\zeta\omega_n\dot{x} + \omega_n^2 x = -\ddot{z}(t) \qquad \text{(B-4)}$$

If an attempt is made to reduce (B-3) to a similar form, the result is

$$\ddot{y} + 2\zeta\omega_n\dot{y} + \omega_n^2 y = \frac{P(t)\omega_n^2}{k} \qquad \text{(B-5)}$$

The following definitions are made: $\delta = 1\#/k$, $P(t)/1\# = g(t)$, and $y/s = u$. Then, (B-5) can be written

$$\ddot{u} + z\zeta\omega_n\dot{u} + \omega_n^2 u = g(t)\omega_n^2 \qquad \text{(B-6)}$$

The shock spectra presented in the earlier portion of this report

are plots of maxi-max values of u. To convert these to displacements $y = u\delta$ where δ is the static displacement due to a one pound load.

APPENDIX C

IMPULSE RESPONSE OF A BERNOULLI-EULER BEAM

The equation of motion of a Bernoulli-Euler beam as shown in Figure 24 is

$$EI \frac{\partial^4 y}{\partial x^4} + \mu \frac{\partial^2 y}{\partial t^2} = 0 \qquad \text{(C-1)}$$

For a hinged-hinged beam, the mode shape is

$$\Phi_n(x) = \text{Sin} \frac{n\pi x}{\ell} \qquad \text{(C-2)}$$

Solution of the form

$$y = \sum_n \Phi_n(x) q_n(t) \qquad \text{(C-3)}$$

is assumed for the forced vibration problem.

For a triangular pulse P(t) of maximum force P_o and duration t_o, as shown in Figure 24, applied at $x = \ell/2$, the bending moment at the center of the beam is

$$M = \sum_{n=1,3}^{\infty} \frac{2P_o\ell}{n^2\pi^2} \left[\left(1 - \frac{t}{t_o}\right) - \text{Cos } \omega_n t_o + \frac{1}{\omega_n t_o} \text{Sin } \omega_n t_o\right]$$

$$\text{for } 0 \leq t \leq t_o$$

$$\text{and} \quad M = \sum_{n=1,3}^{\infty} \frac{2P_o\ell}{n^2\pi^2} \left[A_n \text{Cos } \omega_n(t - t_o) + C_n \text{Sin } \omega_n(t - t_o)\right]$$

$$\text{for } t \geq t_o$$

$$A_n = \left[-\text{Cos } \omega_n t_o + \frac{1}{\omega_n t_o} \text{Sin } \omega_n t_o\right]$$

$$C_n = \left[-\frac{1}{\omega_n t_o} + \text{Sin } \omega_n t_o + \frac{1}{\omega_n t_o} \text{Cos } \omega_n t_o\right]$$